TWO-DIMENSIONAL FINITE ELEMENT ANALYSIS FOR TOOL DESIGN IN ECM

by

K. RAVI RAJU

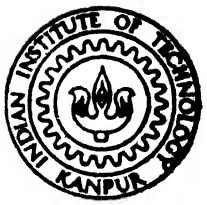

DEPARTMENT OF MECHANICAL ENGINEERING

INDIAN INSTITUTE OF TECHNOLOGY, KANPUR

MARCH, 1987

TWO-DIMENSIONAL FINITE ELEMENT ANALYSIS FOR TOOL DESIGN IN ECM

A Thesis Submitted
In Partial Fulfilment of the Requirements
for the Degree of

MASTER OF TECHNOLOGY

by

K. RAVI RAJU

to the

DEPARTMENT OF MECHANICAL ENGINEERING

INDIAN INSTITUTE OF TECHNOLOGY, KANPUR

MARCH, 1987

25/2/87.

CERTIFICATE

Certified that this thesis work entitled "TWO-DIMENSIONAL FINITE ELEMENT ANALYSIS FOR TOOL DESIGN IN ECM" submitted by Sri K. Ravi Raju in partial fulfilment of the requirements for the degree of Master of Technology of the Indian Institute of Technology, Kanpur is a record of bona-fide research work carried out by him under our supervision and guidance. The work embodied in this thesis has not been submitted elsewhere for a degree.

(G. K. LAL)
Professor
Dept. of Mech. Engg.
I.I.T., Kanpur

(V. K. JAIN)
Assistant Professor
Dept. of Mech. Engg.
I.I.T., Kanpur

ACKNOWLEDGEMENTS

I express my deep sense of gratitude to Dr. V.K. Jain, for suggesting the problem and supervising the work. I am deeply indebted to him for his inspiring guidance, meticulous attention, constructive criticism and above all for his untiring devotion throughout the tenure of this work.

I am grateful to Dr. G.K. Lal for his invaluable advice and suggestions.

I am thankful to Dr. T. Sundararajan for his invaluable suggestions during different stages of this work.

Thanks are due to my friends, Siva Ram, Ramana Murthy, Kiran and Ramana for their nice company during the stay in IIT Kanpur.

I am thankful to Mr. R.N. Srivastava for his excellent and neat typing.

Finally, I wish to thank my wife, Mrs. Suneetha Ravi, for her encouragement throughout the course of this work.

K. Ravi Raju

CONTENTS

LIST OF TABLES

LIST OF FIGURES

NOMENCLATURE

A	Atomic weight of the work material
A_r	Area
b_b	Bare length of the electrode (or height of the bit)
$[B]$	Boundary matrix
C_p	Specific heat of electrolyte
C_{PL}	Specific heat at constant pressure
D	Hydraulic mean diameter
E	Electrochemical equivalent
E_v	Effective voltage
f	Feed rate
f_n	Feed rate vector normal to the work surface
F	Faraday's constant
h	Convective heat transfer coefficient
I	Current
INM	Last node in the front zone
J	Current density
K	Electrolyte conductivity
$[K_s]$	Thermal stiffness matrix
KIN	An index used to count the number of computational cycles
L	Length of the workpiece
N_i	Interpolating function/shape function
$N_{,x}$, $N_{,y}$	Derivatives of interpolating constants
n	Void fraction exponent
P	Electrolyte pressure in the IEG
q	Heat transferred

Q	Discharge of electrolyte
$\dot{H}$	Rate of heat generation per unit volume
R_g	Gas constant
R_e, R	Electrical resistance
R_n	Reynold's number
r, R	Radius
r_1	Inner radius of the tool
r_2	Outer radius of the tool
R_{a1}	Work corner radius
R_{a2}	Tool corner radius
t	Time
T	Temperature
U	Electrolyte flow velocity
V	Applied voltage
W	Width of workpiece
X	Distance along electrolyte flow direction (x coordinate)
Y	Coordinate measured in y direction (interelectrode gap)
Z	Valency of electrochemical dissolution
α	Temperature coefficient of electrolyte conductivity
α_v	Void fraction coefficient
Δ^e	Area of the element
Δt	Computational cycle time
ΔT	Incremental change in temperature
ΔV	Over potential
η	Current efficiency or machining efficiency
θ	Angle
ρ	Mass density

σ	Gas slip ratio
τ	Shear stress
μ	Viscosity of the electrolyte
ϕ	Electric field potential

SUBSCRIPTS

a	Anode
b	Boring
d	Drilling
e	Electrolyte, element, equilibrium
g	Gas
i	Inlet condition
i, j	Node number
o	Initialcoonditions, condition at inlet
v	Volumetric
w	Work material

SUPERSCRIPTS

e	Element
ne	Nodes at an element

ACRONYMS

BEM	Boundary element method
FDT	Finite difference technique
FEM	Finite element method
IEG	Interelectrode gap
MRR	Metal removal rate
OWS	Obtained work shape
RWS	Required work shape

ECD	Electrochemical drilling
ECB	Electrochemical boring
ECBD	Electrochemical bit drilling
ECBB	Electrochemical bit boring

ABSTRACT

Electrochemical machining (ECM) is one of the most widely used unconventional manufacturing process. Its capabilities have not been fully exploited mainly due to some inherent problems associated with tool design. Conventional ECM tool design is not accurate enough to account for different complex phenomenon taking place in interelectrode gap. One such phenomenon is heat transfer through the electrodes. There is no accurate model available for the heat transfer analysis of ECM.

In the present work, a two-dimensional, unsteady state heat transfer model has been proposed to analyze the heat transfer from electrolyte to and through the electrodes, for obtaining the temperature distribution in interelectrode gap. Experimental data have been used to test the accuracy of the model. Comparison of analytical and experimental temperature distribution reveals a good agreement between the two. It has been concluded that the anode shape can be predicted more accurately by incorporating two-dimensional, unsteady state heat transfer.

Majority of the models available for tool design in ECM ignore the effect of variation in different process parameters. A method has been suggested for the determination of the shape of the tool (cathode) to produce the required work (anode) shape, while machining under specified machining conditions. This method takes into account the effect of variation in different process parameters. The cathode shape prediction problem has been attempted for electrochemical drilling with a bare tool, electrochemical bit drilling and electrochemical bit boring. Tools and tool bits have been designed for producing profiles obtained experimentally and also for producing straight sided holes. Comparison of designed and experimental tool shapes reveals a good agreement between the two.

CHAPTER I

INTRODUCTION AND LITERATURE SURVEY

1.1. ELECTROCHEMICAL MACHINING (ECM):

The rapid developments in the field of materials have given an impetus to the modern manufacturing technology to develop, modify and discover newer technological processes with a view to achieve results that are far beyond the scope of existing conventional or traditional manufacturing processes. As a result of such developments in the field of materials, some new techniques of machining such as ECM, EDM, USM, AJM, EBM, etc., have been developed. These nontraditional processes are capable of providing effective solutions to the problems imposed by the increasing demand for accurate machining of high-strength-temperature-resistant (HSTR) alloys, the requirements of parts with intricate and complicated shapes, and materials so hard as to defy machining by conventional methods.

Electrochemical machining (ECM) is one of the most widely used unconventional machining process. ECM is a process of controlled and accelerated anodic dissolution of metals and alloys. High velocity electrolyte flows between anode and cathode (Figure 1.1) subjected to a small d.c. voltage and maintaining a small interelectrode gap (IEG) between them. The flowing electrolyte helps not only in allowing the high rate of metal dissolution, but also takes away the reaction products and heat generated during the chemical and electrochemical reaction.

The beauty of ECM process is its ability to machine very hard metals without causing and tool wear, high metal removal rate, no structural damage to the workpiece and to machine complex shapes with good surface finish that too in single stage. The different fields of applications [1] of ECM are drilling, boring, turning, cavity sinking, milling, grinding, deburring, polishing etc. However, the capabilities of such a high potential process have not been fully exploited because of lack of understanding of the mechanism of metal removal and inexistence of an efficient tool design methodology.

ECM is a highly complex phenomenon. Most of the machining parameters such as, electric field distribution, electrolyte conductivity (K), gas evolution, temperature rise (ΔT), valency of dissolution (Z), electrolyte flow velocity (U), etc., are simultaneously and continuously varying along the electrolyte flowpath and with the machining time. Their interaction is of complex nature and there is a lack of clear understanding of the mechanism of metal removal. Further, the electrolyte in the gap is a mixture of evolved gases (such as hydrogen, oxygen and chlorine), solids and precipitates. In majority of the cases, IEG is complex shaped and it is difficult to evaluate flow parameters since there are electrolyte starvation, and cavitational effects as well.

1.2. TOOL (CATHODE) DESIGN FOR ECM

Tool design in ECM deals with the computation of tool shape which under specified machining conditions would produce a work having a prescribed shape or profile accurately.

Alternatively, it also deals with the production of work shape obtainable from a tool of known geometry when machining is performed under specified machining conditions.

There are two main aspects in the design of tools for ECM [2]. First is the determination of the shape of the tool together with the optimum machining conditions [3] necessary to produce the required work shape. The second aspect is a practical one, which is concerned with making the tool of the appropriate material, fixing it in the machine, connecting it to the power supply, arranging an adequate supply of electrolyte between tool and workpiece and insulating parts of the tool or to use bit type of tool to prevent machining in undesired regions. The design requirements for some of these aspects may be conflicting and many of them may make it necessary to modify the tool geometry. Here, only the first aspect of tool design is dealt with prescribed machining conditions have been used for cathode shape design.

In general, cathode design for ECM is based on the 'trial and error' method which also involves actual machining. Such practical methods of obtaining tool shape are expensive, time consuming and inaccurate. The analytical design of ECM tools is complicated on account of complexity of interaction between simultaneously and continuously varying machining parameters. Several attempts have been made to develop a comprehensive model of the mechanics of metal removal in ECM, particularly with the view of developing an accurate method for tool design. Some of the models for anode shape prediction and cathode shape design have been discussed below.

1.3. COSΘ METHOD

Tipton [4, 5] attempted tool design for ECM by using cosΘ method, with the assumption that the electric flow lines are straight and normal to the work surface. In this method, equilibrium work shape is computed corresponding to the tool whose profile has to be approximated by large number of planar sections inclined at different angles, as shown in Figure 1.2.

For plane parallel electrodes with their surfaces normal to the direction of feed, the equilibrium gap, Y_e, is given by equation (1.1)

$$Y_e = \frac{K(V - \Delta V)E}{F \rho_w f} \qquad (1.1)$$

The equilibrium gap between any section of cathode surface and that corresponding surface of the anode which is parallel to it is given by $Y_e/\cos\Theta$. The angle 'Θ' is measured between normal to the anode surface and the direction of the cathode feed. The cathode shape for a given anode shape can be computed from the following parametric equations.

Suppose the anode shape is given by,

$$Y = f(X) \qquad (1.2)$$

Any point, say A(X, Y), on the anode surface corresponds to an equivalent point $B(X_1, Y_1)$ on the cathode surface. The gap width between A and B then becomes $Y_e/\cos\Theta$ (Figure 1.2), we have,

$$Y - Y_1 = AB \cos\Theta = Y_e \qquad (1.3)$$

and

$$X_1 - X = AB \sin\theta = Y_e \tan\theta$$

$$= Y_e\left(\frac{dY}{dX}\right) \qquad (1.4)$$

By substituting the values of X and Y from equations (1.3) and (1.4) in equation (1.2), gives an equation for the cathode surface [1].

The 'cosθ' method is generally applicable to the regions where the local radii of curvature of the anode and cathode surfaces are large compared with the equilibrium gap. This method excludes the effect of different process parameters on predicted anode profile. Workpieces having sharp corners and complex shapes cannot be analysed with this method.

1.4. NUMERICAL METHODS

In ECM, the change in shape of the workpiece during machining depends on the local current density, which in turn changes with the changing work shape. To determine current density, it is necessary to solve Laplace equation for the field distribution in the IEG. With the availability of high speed computers, numerical methods for solving Laplace equation have been developed.

1.4.1. FINITE DIFFERENCE TECHNIQUE (FDT)

Tipton [5] and Hopenfield and Cole [6] applied FDT to determine potential distribution in the IEG for non-passivating electrolyte assuming constant conductivity and temperature.

Figure 1.3(a) shown the tool work surfaces and IEG drawn in square meshes containing a set of grid points of

general co-ordinates (i, j). The potential values for the grid points on the cathode boundary are assigned zero, and those on the anode boundary are set to some known values. The initial potential at the grid points within the IEG region are set by linear interpolation along the vertical grid lines between anode and cathode. These values must be progressively adjusted until they satisfy a finite difference equation corresponding to Laplace's equation in the region between the boundaries.

For a point 'o' located in a mesh of spacing h(i, j), the finite difference equation corresponding to Laplace's equation becomes,

$$\frac{\partial^2 \phi}{\partial x^2} + \frac{\partial^2 \phi}{\partial y^2} = 0 \qquad (1.5)$$

Using eq. (1.2), eq. (1.3), can be obtained for calculating the potential at 'o'

$$\phi(i, j) = \frac{(\phi_{i+1,j} + \phi_{i-1,j} + \phi_{i,j+1} + \phi_{i,j-1})}{4} \qquad (1.6)$$

In some cases, all points on the anode and cathode boundary may not lie on grid points. In such cases, it is customary to relax the potential by linear interpolation.

1.4.2. FINITE ELEMENT METHOD (FEM)

In case of complex shaped IEG, the cathode and anode boundaries cannot be matched accurately using square meshes, which introduce further approximations. In order to overcome

these approximations, Jain and Pandey [7] suggested FEM which can be applied to analyse any complex shaped IEG.

Jain [8] has developed FEM models, FET11 and FET22, for the prediction of anode profiles in the case of plane parallel machining. The model FET11 is based on the Ohm's law for the calculation of current densities in the IEG and FEM has been applied to obtain temperature distribution within the IEG. In the model FET22, Laplacian equation has been solved to obtain potential distribution within the IEG from which current densities are calculated. Jain also extended the model FET11 (Model SGFET11) for predicting the anode profile in case of rectangular and cylindrical deep hole drilling operations. All these models are capable to predict the anode shape accurately, by taking into consideration, the variations in different process parameters. A new concept of ECM tools was introduced by Jain [9, 10]. Murugan [11] and Yogindra [12] have extended FEM models for anode shape prediction using bit type of tools.

1.4.3. BOUNDARY ELEMENT METHOD (BEM)

Both the methods FDT and FEM yield solutions corresponding to internal as well as boundary nodes, but in most cases (like in ECM) internal solutions are unnecessary. In BEM, boundary alone is discretized into segments. It considerably reduces both the amount of input data and its preparation time. The solutions are predominently boundary based but solutions to internal points can be obtained.

Narayananan, Hinduja and Noble [13] have applied BEM, for the anode shape prediction in ECM. Linear and quadratic

elements were used to represent the boundaries. It was concluded that comparatively better accuracy was obtained by using BEM, with far less computational effort.

1.5. CATHODE SHAPE PREDICTION BY DRAWING CURVILINEAR SQUARES IN THE IEG

Tipton [5] has developed a method of determining the tool shape by drawing curvilinear squares between the work and tool boundaries. It defines the work surface numerically in X, Y plane with Y as feed direction and with coordinates spaced by constant X increment equal to a fraction of the equilibrium gap. In the equilibrium condition, the normal current density is constant, so that a constant current increment I flows between each of the adjacent coordinates on the work boundary because they are equally spaced in the X-direction. The work boundary is assumed to be equipotential and each coordinate represents the end of a current flow line. By using each adjacent pair of coordinates, it is possible to draw the curvilinear squares and to construct the first row of potential field distribution between the work and tool as shown in Figure 1.4. If the X coordinate spacing is Y_e/n then repetition of the process will produce the nth equipotential which is a tool surface. Each of the intermediate surfaces is also a tool surface for equilibrium gaps of Y_e/n, $2Y_e/n$, $3Y_e/n$, etc.

The process of drawing curvilinear squares is based on differentiating the input data. Differentiation is a noisy process, which magnifies random error in the data, specially when the process is repeated several times. Complete failure of calculation occurs when two current flow lines cross each

other. In that case, the previous equipotential could be used as tool with the corresponding fractional equilibrium gap. In this model, variations in all the process parameters have not been taken into account.

1.6. COMPLEX VARIABLE TECHNIQUE

Wilson and Tusei [14, 15], used complex variables technique to solve the field equation in IEG. The tool design problem was formulated as an inverted Cauchy problem, in which the spatial coordinates were treated as the dependent variables on the plane of the complex potential [15]. The equations of equipotential lines are directly obtained for a given work profile [14], which define the equation for a family of tool curves. Limitation of the above method is that it can be used only for analytic work surfaces, i.e. this method cannot be used for discontinuties in derivatives of work and tool surfaces. It needs a lot of mathematical analysis.

1.7. CONTINUITY METHOD

Lawrence [16] developed a graphical technique for tool design by solving the field equation in the gap. But this procedure gives low accuracy and it is more tedious. He subsequently adopted numerical methods to solve the field equation using digital computer. In this method, starting from a defined equipotential work shape boundary, a model of electric field is constructed, where each new equipotential surface is a possible tool shape which will produce the original work shape. This method rests on the assumptions that Ohm's law applies across a

small element of electrolyte and that the current flowing between a pair of flux lines in an electric field is constant. It does not account for the variation in electrolyte parameters in the IEG.

1.8. HEAT TRANSFER IN ECM PROCESS

During ECM, a large amount of heat is generated in IEG by different sources of heat viz., Ohmic resistance of electrolyte, reversible and irreversible chemical reactions, viscous flow of electrolyte etc. A major contribution is by the Ohmic heating of the electrolyte [17]. But a significant amount of heat is transferred to the surrounding atmosphere through the electrodes. This lowers down the temperature of the electrolyte, hence it becomes essential to incorporate the effect to modify the electrolyte conductivity along the flow path to get accurate results. Apart from the conductivity, change in electrolyte temperature affects the other machining parameters also. Heat transfer analysis in ECM is quite complicated and involves multiphase turbulent flow with heat generation between the electrodes. In majority of the models for ECM tool design, therefore, heat transfer through the electrodes has been neglected. This leads to poor correlation between analytical and experimental results.

1.8.1. THERMAL RESISTANCE MODEL

Jain and Pandey [18] have suggested a simplified, unidimensional thermal resistance model for heat transfer analysis of ECM. For an IEG system, temperature gradient and simplified thermal resistance model [18] are shown in Figures

1.5(a) and 1.5(b) respectively. The drop in temperature of the electrolyte due to transfer of heat to the atmosphere is evaluated using the following equation,

$$q = q_a + q_c$$

where q_a = heat transferred from anode to the air

and q_c = heat transferred from cathode to the air.

But this method is based on the following assumptions:

1. IEG system behaves like a single phase fluid
2. Heat transfer through electrodes is unidirectional
3. Heat transfer within the IEG occurs under steady state conditions.

Murugan [11, 19] had investigated into the effects of cathode material on temperature distribution during ECM, using the simplified thermal resistance model.

Kawafune, Mikoshiba and Noto [20], analyzed the effect of temperature and other working parameters on the working gap during ECM. In the analysis, an equation for the temperature rise had been derived assuming steady state heat transfer. Also, the physical constants (K, P_r, C_{PL}, γ) of water were used for heat transfer equations instead of those for electrolyte.

1.9. PRESENT WORK.

From the above literature survey it is evident that there is no accurate model available for heat transfer analysis of ECM. The work embodied in the first part of this thesis has been aimed towards the development of a two dimensional, unsteady state heat transfer model to analyze the heat transfer fromth

the electrolyte to and through the electrodes, for obtaining the temperature distribution in the IEG. The anode shape prediction model (FET22) for plane parallel electrodes ECM developed by Jain [8], has been modified by incorporating the two-dimensional, unsteady state heat transfer. It has been named as TFET22.

The analytic temperature distribution, obtained by TFET22, in IEG has been compared with the experimental temperature distribution obtained by Bhatia [21, 22] and with one-dimensional heat transfer analytical results obtained by Murugan [11].

The second part of the work has been aimed towards the development of a computer aided method for the tool design for ECM. The cathode (tool) shape prediction problem has been attempted for electrochemical drilling with a bare tool, electrochemical bit drilling and electrochemical bit boring. The anode shape prediction model (SBFET22), first developed by Jain [8] and later modified by Yogindra [12], has been used in the design package for ECD and ECBD. The model SBFET22 has been modified for the anode shape prediction for ECB.

Tools and tool bits have been designed for producing profiles obtained experimentally and also for producing straight sided holes, while machining under prescribed machining conditions. Designed tool shapes have been compared with the experimental tool shapes used by Jain [8] for ECD and ECBD.

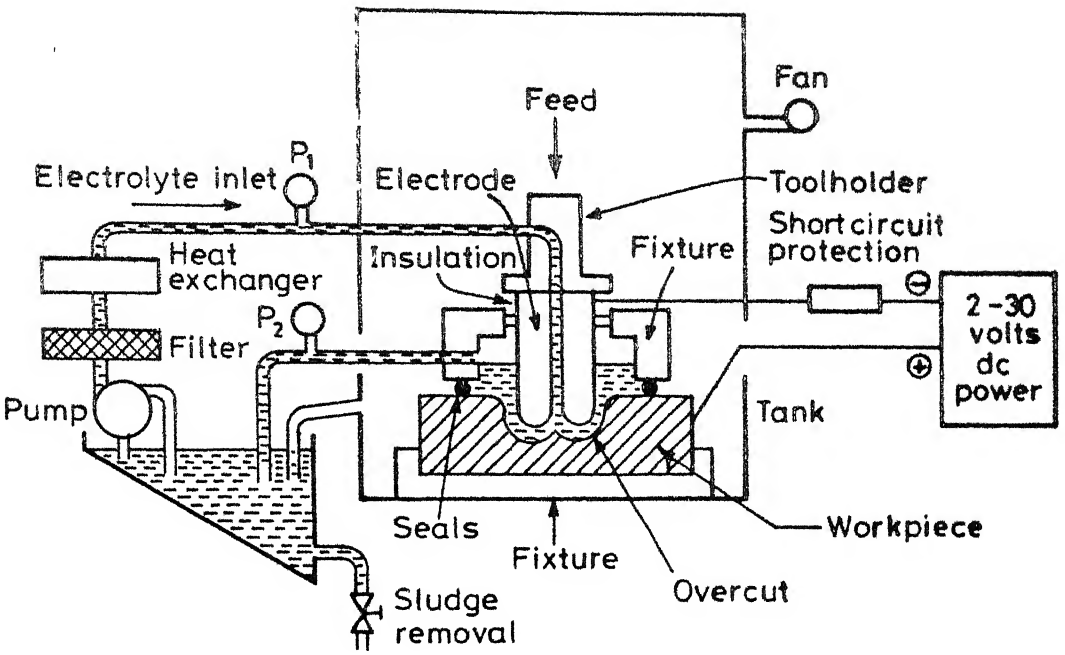

FIG. 1.1 BASIC SCHEME OF ELECTRO-CHEMICAL MACHINING PROCESS.

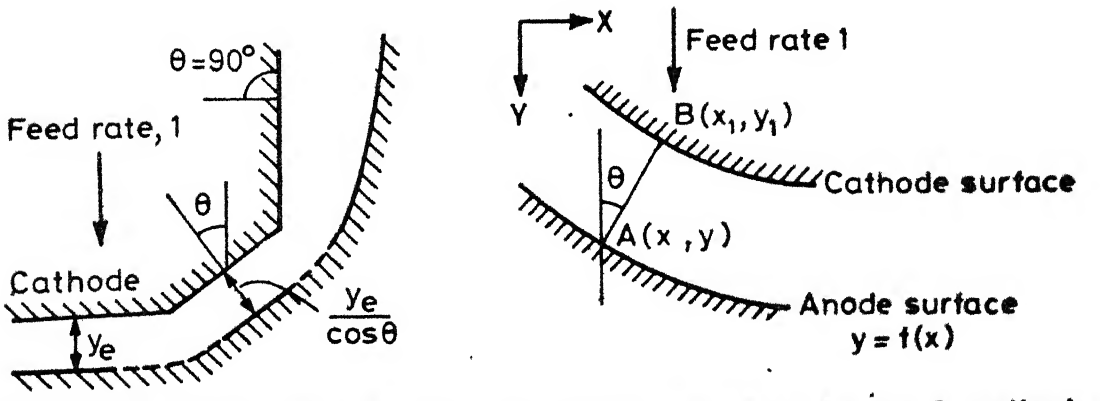

(a) Principle of the cos θ method (b) Cathode design by cos θ methode

FIG. 1.2 Cos θ METHOD

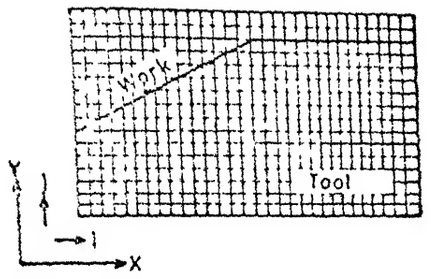

(a) IEG-tool work system discretised in square meshes

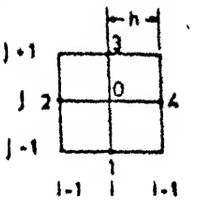

(b) A square mesh of spacing h with general point O(I, J)

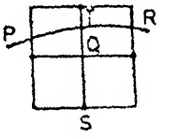

(c). Boundary forms irregular star with one short arm QT.

Fig.1.3 Finite difference technique.

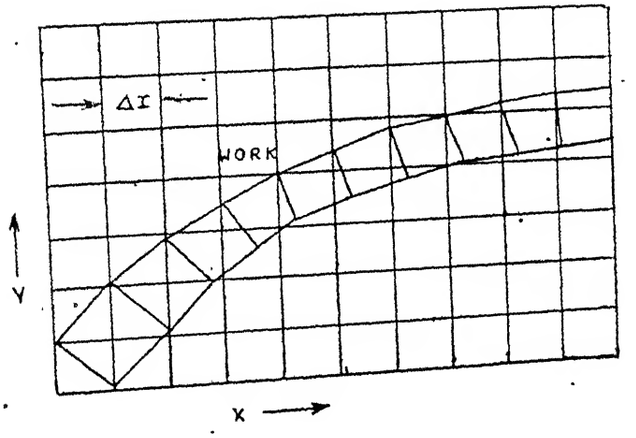

Fig. 1.4 The first step in calculating a tool shape by calculating the field distribution between the work and tool as a series of curvilinear squares.

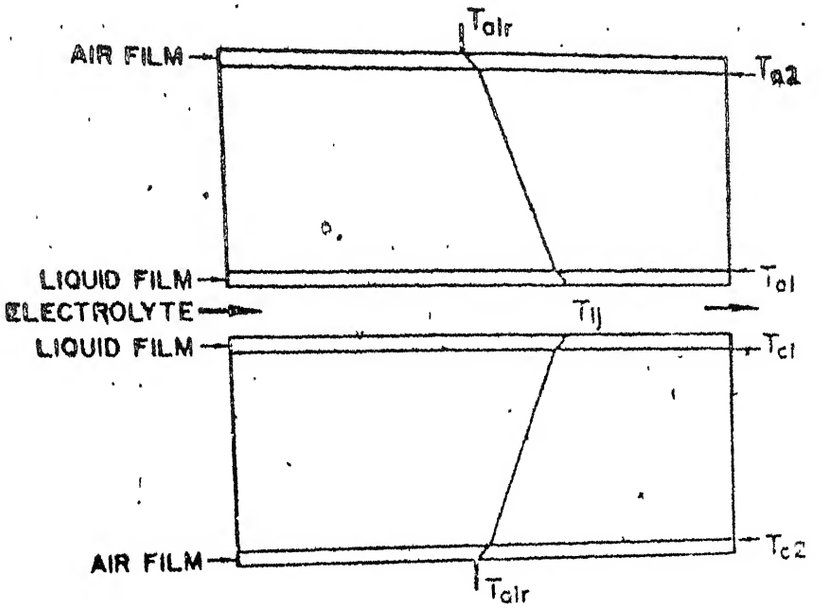

(a)

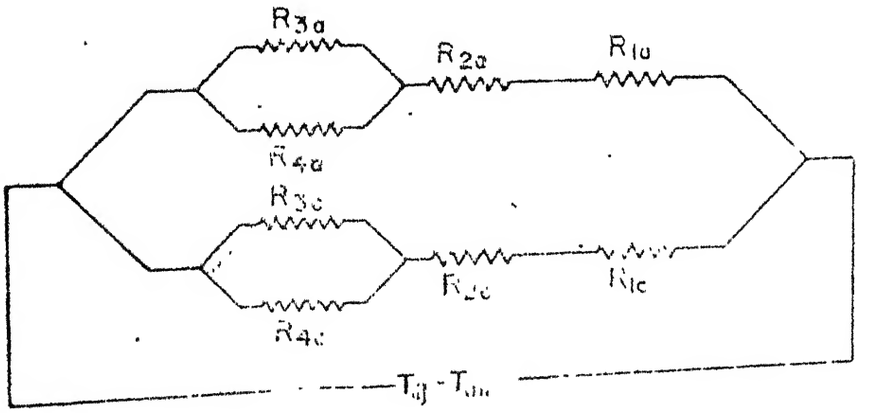

(b).

Fig. 1.5 Thermal resistance model.

CHAPTER II

THEORETICAL ANALYSIS

2.1. INTRODUCTION

In this chapter, ECM with plane parallel electrodes and electrochemical drilling have been analyzed separately. The expressions for various process parameters such as electrolyte conductivity, flow velocity, current density, void fraction, temperature and pressure distributions etc. have been given. All the three zones namely, front, transition and side zones in the case of ECD have been analyzed individually with some suitable assumptions. However, stagnation zone has been ignored.

2.2. ANALYSIS OF ECM WITH PLANE PARALLEL ELECTRODES

2.2.1. ELECTROLYTE FLOW VELOCITY

Assuming uniform velocity distribution across the flow direction, electrolyte flow velocity at any cross section is given by

$$U = \frac{Q}{A} \qquad (2.1)$$

where Q is the discharge and A is the cross sectional area.

2.2.2. CURRENT DENSITY AND CONDUCTIVITY

The current density within the IEG, can be determined either from Ohm's law or from the potential distribution obtained by solving Laplace equation. The application of a particular

case depends upon the nature of the current lines. Ohm's law can be applied only when the current lines are straight and parallel. But this is not true when electrodes with small radii or complex shape are used. In such cases, the current density calculated from the potential distribution obtained by solving Laplace equation gives more accurate results. The current density at any point on the workpiece is calculated as

$$J = K \frac{\partial \phi}{\partial n} \qquad (2.2)$$

The electrolyte conductivity, K, has been known to be a function of both, electrolyte temperature and void fraction. For computation of K, Tipton [4] proposed the equation given below, which accounts for the effects of electrolyte temperature and hydrogen gas liberation:

$$K = K_o [1 + \alpha (\Delta T)] (1 - \alpha_v)^n \qquad (2.2a)$$

In eq. (2.2), Hopenfeld and Cole [6] assumed a value of n = 1.5 for the case of uniform void distribution. For the case of non-uniform void distribution, especially where bubbles are concentrated near the cathode, Thrope and Zerkle [23] suggested a value of n = 2.0.

2.2.3. CURRENT EFFICIENCY

In deriving the expression for metal removal rate (MRR) by Faraday's laws of electrolysis, current efficiency was assumed to be 100%. But in the actual machining process, it depends on the current efficiency achieved [1], i.e., the

proportion of the total current that is used for the removal of metal from the anode. The current efficiency is given by

$$\eta = \frac{\text{Actual metal removed}}{\text{Theoretical metal removed}} \times 100\% \qquad (2.3)$$

In actual practice, the values of current efficiency may be higher or lower than 100%, depending on the conditions of machining. Current efficiency values less than 100% are obtained because of the occurrence of the side reactions at the anode, e.g., evolution of oxygen gas or Fe^{+++} ions instead of Fe^{++} ions etc.

If the dissolution of the anode occurs at a valency lower than the one used during calculation, the current efficiency obtained may be higher than 100%. Moreover, selective machining may occur at the material irregularities, such as at the grain boundaries and hence may cause chunks of material to be removed. In this case, the actual material removed is more than the theoretical which results in current efficiency higher than 100%.

2.2.4. INTERELECTRODE GAP (IEG)

EC reactions would attain an equilibrium only after time t approaches infinity and IEG can be computed from equations (2.4) and (2.5) while machining with zero and finite feed rates [1] respectively,

$$Y = (Y_o^2 + 2ct)^{1/2} \qquad (2.4)$$

where $c = \frac{\Lambda K(V - \Delta V)}{Z \rho_w F}$

and

$$t = \frac{1}{f}(Y_o - Y) + \ln\left(\frac{Y_o - Y_e}{Y - Y_e}\right) \qquad (2.5)$$

Equation (2.5) is an implicit equation and can be solved by iteration process. Equation (2.4) predicts an infinite value of the gap as 't' approaches infinity. However, in practice, as the IEG increases, the current density decreases, so that the MRR gradually decreases and for a very large gap, the process would come to a stand still.

For a very small interval of time Δt, Jain and Pandey [7, 10] derived an eq. (2.6) for determining IEG which holds good for both, zero and finite feed rate.

$$Y = Y_o + (c' - f)\Delta t \qquad (2.6)$$

where $c' = \frac{\eta J A}{\rho_w F Z}$

Equation (2.6) is based on the assumption that the current density 'J' remains constant over a small element of length dX and for a small interval of time, Δt. This equation yields values of Y which are close to those obtained from eqs. (2.4) and (2.5) and agree well with experimental data [8]. In the present work eq. (2.6) has been used.

2.2.5. TEMPERATURE

Following assumptions are made in deriving the equations for temperature distribution:

(1) Total heat generated is only due to Ohmic heating (i.e. I^2R_e). The heat generated by other sources is negligible [1].

(2) Specific heat and density of the electrolyte remain constant in IEG.

(3) Heat transfer through the electrodes is considered to be negligible i.e., all the heat generated is retained by the electrolyte.

Consider an element of length dy and width 'B' in the IEG (Figure 2.1).

The mass of the electrolyte flowing

across the element per unit time = $y\ B\ U\ \rho_e$

$= Q\ \rho_e$

Heat carried away by the electrolyte

$$= y\ B\ U\ \rho_e\ c_e \qquad (2.7)$$

Heat generated in the element,

$$dH = I^2 R_e = \frac{B(V - \Delta V)^2}{y} K_o [1 + \alpha \Delta T]\ dx \qquad (2.8)$$

Equating eqs. (2.7) and (2.8) and separating the variables, gives

$$\frac{dT}{1 + \alpha(T - T_i)} = \frac{K_o (V - \Delta V)^2}{y^2\ U\ \rho_e\ c_e}\ dx \qquad (2.9)$$

The integration of the above equation with boundary conditions at $x = 0$, $T = T_i$ gives

$$(T - T_i) = \frac{1}{\alpha}\left\{\exp\left[\alpha\ \frac{K_o (V - \Delta V)^2 x}{y^2\ \rho_e\ c_e\ U}\right] - 1\right\} \qquad (2.10)$$

2.3. ANALYSIS OF EC DRILLING

2.3.1. ELECTROLYTE FLOW VELOCITY

In the present case, the mode of electrolyte flow is outward and separate expressions have to be derived for front,

side and transition zones. The assumptions made are,

(1) The volume of electrolyte flowing at any section per unit time is constant.

(2) Cavitation and starvation of the electrolyte are neglected.

(3) Electrolyte velocity across the flow direction is assumed to be uniform.

FRONT ZONE

In this zone, electrolyte flows in radial direction. Electrolyte flow velocity at any radius (Figure 2.2) from the axis of the tool is given by

$$U = \frac{Q}{A_r} = \frac{Q}{2\pi r Y} \qquad (2.11)$$

where Q = discharge of electrolyte.

TRANSITION AND SIDE ZONES

As the tool corner radius is very small electrolyte flow in both the zones is assumed to be in axial direction. From Figure 2.2

$$A_r = \pi(r_2 + Y)^2 - \pi r_2^2$$

$$= \pi(Y^2 + 2r_2 Y) \qquad (2.12)$$

and

$$U = \frac{Q}{\pi(Y^2 + 2r_2 Y)} \qquad (2.13)$$

2.3.2. CURRENT DENSITY AND CONDUCTIVITY

These are evaluated in the same way as discussed earlier in the case of ECM with plane parallel electrodes.

2.3.3. TEMPERATURE

By making the same assumptions as in the case of plane parallel electrodes BCM, the expressions for temperature distributions have been obtained as follows.

FRONT ZONE

Consider an element of thickness 'dr' at a distance, r, from the axis of the tool (Figure 2.2).

Using Ohm's law, it can be shown that the current I through this element is given by

$$I = \frac{K(V - \Delta V)\, 2\pi r\, dr}{Y} \qquad (2.14)$$

Heat generated in the element,

$$dH = I^2 R_e = \frac{K(V - \Delta V)^2\, 2\pi r\, dr}{Y} \qquad (2.15)$$

Heat carried away by the electrolyte,

$$dH = Q\, \rho_e\, c_e\, dT \qquad (2.16)$$

Equating (2.15) and (2.16) yields

$$Q\, \rho_e\, c_e\, dT = \frac{(V - \Delta V)^2\, K\, 2\pi r\, dr}{Y} \qquad (2.17)$$

Using $K = K_o(1 + \alpha \Delta T)$, the expression for temperature distribution becomes,

$$\frac{dT}{1 + \alpha(T - T_i)} = A^* r\, dr \qquad (2.18)$$

where, $A^* = \dfrac{2\, K_o (V - \Delta V)^2}{Q\, \rho_e\, c_e\, Y}$

The integration of eq. (2.18) with boundary condition at $r = r_i$, $T = T_i$ gives,

$$T - T_i = \frac{1}{\alpha} \exp\left[A^* \frac{(r^2 - r_i^2)}{2} \right] - 1 \qquad (2.19)$$

TRANSITION AND SIDE ZONES

In these zones, the electrolyte flow is assumed to be in axial direction. Consider an element of length dX at a distance X from the end of the front zone, i.e., from X_{ref} (Figure 2.2).

By Ohm's law,

$$I = \frac{(V - \Delta V) K \, 2\pi (r_2 + Y) dX}{Y} \qquad (2.20)$$

From eq. (2.20) the heat generated in the element is given by

$$dH = I^2 R_e = \frac{(V - \Delta V)^2 K \, 2\pi (r_2 + Y) dX}{Y} \qquad (2.21)$$

Equating eqs. (2.16) and (2.21) gives

$$Q \rho_e c_e \, dT = \frac{(V - \Delta V)^2 \, K \, 2\pi (r_2 + Y) dX}{Y} \qquad (2.22)$$

or $$\frac{dT}{1 + \alpha (T - T_i)} = A' \, dX$$

where,

$$A' = \frac{2\pi K_o (V - \Delta V)^2 (r_2 + Y)}{Q \rho_e c_e Y} \qquad (2.23)$$

Integrating eq. (2.23) with boundary condition, i.e., at $x = X_{ref}$, $T = T_{ref}$ gives

$$(T - T_i) = \frac{1}{\alpha} \left[B \exp\left[\alpha A' (X - X_{ref}) \right] - 1 \right] \qquad (2.24)$$

where,

$$B = 1 + \alpha (T_{ref} - T_i) \qquad (2.25)$$

2.3.4. VOID FRACTION (α_v)

During high current electrolysis, hydrogen will evolve at anode and oxygen at the cathode. Hopenfeld and Cole [6] are of the opinion that the amount of oxygen is too small for realistic considerations. Similarly, the presence of chlorine can be neglected due to its solubility in water. Hence, for void fraction calculation, the effect of hydrogen is considered.

Considering a control volume in IEG (Figure 2.3), using the principle of conservation of mass, Thrope and Zerkle [23] arrived at the governing nonlinear differential equation and the expression for void fraction was obtained by solving it, as follows

$$\alpha_v = \frac{B^* X^*}{1 + B^* X^*} \qquad (2.26)$$

where, $B^* = \dfrac{\rho_e E_g}{\sigma \rho_g E_a}$

$$X^* = \frac{X}{LS} \quad \text{(for rectilinear flow)}$$

$$= \frac{X(r_i + X/2)}{L S r_i} \quad \text{(for radial flow)}$$

$$S = \frac{\rho_i Y_i U_i}{L \rho_a f}$$

In the present case, the gas slip ratio σ in the variable B^* is assumed to be unity, that is, velocity of gas is same as that of velocity of the electrolyte.

2.3.5. ELECTROLYTE PRESSURE

The electrolyte pressure (P) required to maintain the rate of electrolyte flow in a particular gap is given by

$$P = P_1 + P_2 \qquad (2.27)$$

where P_1 is the pressure required to overcome inertia force and P_2 is the pressure required to overcome viscous force. The expressions for P_1 and P_2 are different for laminar and turbulent flows. The type of flow in the IEG can be determined from Reynold's number and is given by the eq. (2.28)

$$R_n = \frac{\rho_e U_e D}{\mu_e} \qquad (2.28)$$

where D = The hydraulic mean diameter

$$= \frac{4 \times \text{Area of cross section}}{\text{Wetted parameter}}$$

= d for a cylindrical tube

= $(d_1 - d_2)$ for the case in which fluid is flowing through the annulus

= 2Y for a rectangular channel of depth Y.

For the laminar flow ($R_n < 2000$) with a parabolic velocity distribution, the pressures P_1 and P_2 are given by

$$P_1 = \frac{1}{2} \rho_e U_e^2$$

and

$$P_2 = \frac{32 \mu_e U_e X}{d^2} \quad \text{for a narrow tube of diameter d} \qquad (2.29)$$

The flow is usually turbulent ($R_n > 2000$) in ECM. From Bernouli's equation,

$$P_1 = \frac{1}{2} \rho_e U_e^2 \qquad (2.30)$$

The value of P_2 is given by Blasius ecuation

$$P_2 = \frac{0.3164 \rho_e U_e^2 K}{2n R_n^{0.25}}$$

The pressure P_2, in turbulent flow is a function of Reynold's number. At high Reynold's number inertia force will be more than the viscous force which results in higher value of P_1.

2.3.6. IEG

IEG is calculated in the same way as discussed earlier in the case of ECM with plane parallel electrodes.

2.3.7. FEED RATE IN TRANSITION AND SIDE ZONES

In EC drilling, as the machining progresses, the side zone becomes tapered and it no longer remains zero feed rate case. For the calculation of IEG in the side zone, the feed rate vector normal to the work surface should be considered, as given by eq. (2.31)

$$f_n = f \cos\theta \qquad (2.31)$$

where θ is the angle of inclination between the feed direction and normal to the work surface. The values of 'θ' for each element in side zone and transition zone are calculated separately.

If Y_1 and Y_2 are the interelectrode gaps, say in side zone at points 1 and 2 respectively (Figure 2.4) then the angle θ at the point 2 is given by

$$\theta = \tan^{-1} \left(\frac{X_2 - X_1}{Y_2 - Y_1} \right)$$

In the transition zone, the angle θ at any point is given by the intersection angle between the normal drawn at a point and the tool feed direction (Figure 2.4).

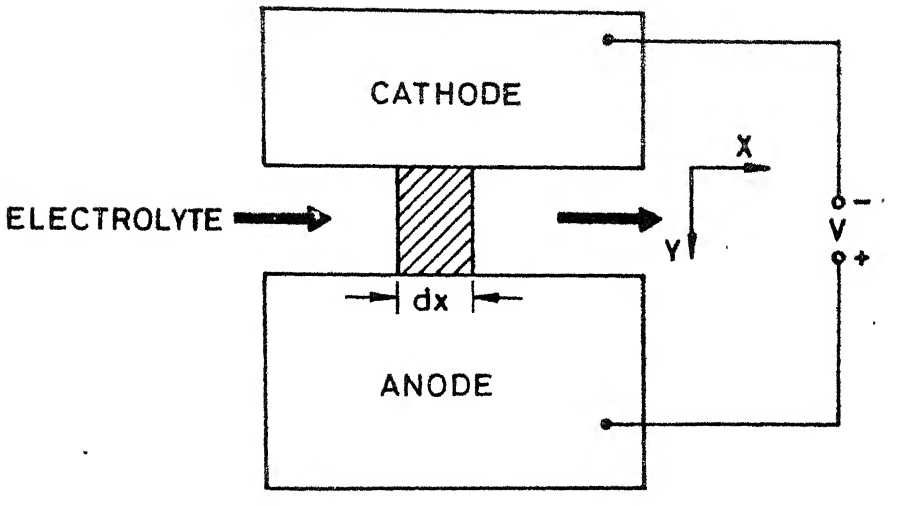

FIG. 2.1 PLANE PARALLEL ELECTRODES ECM.

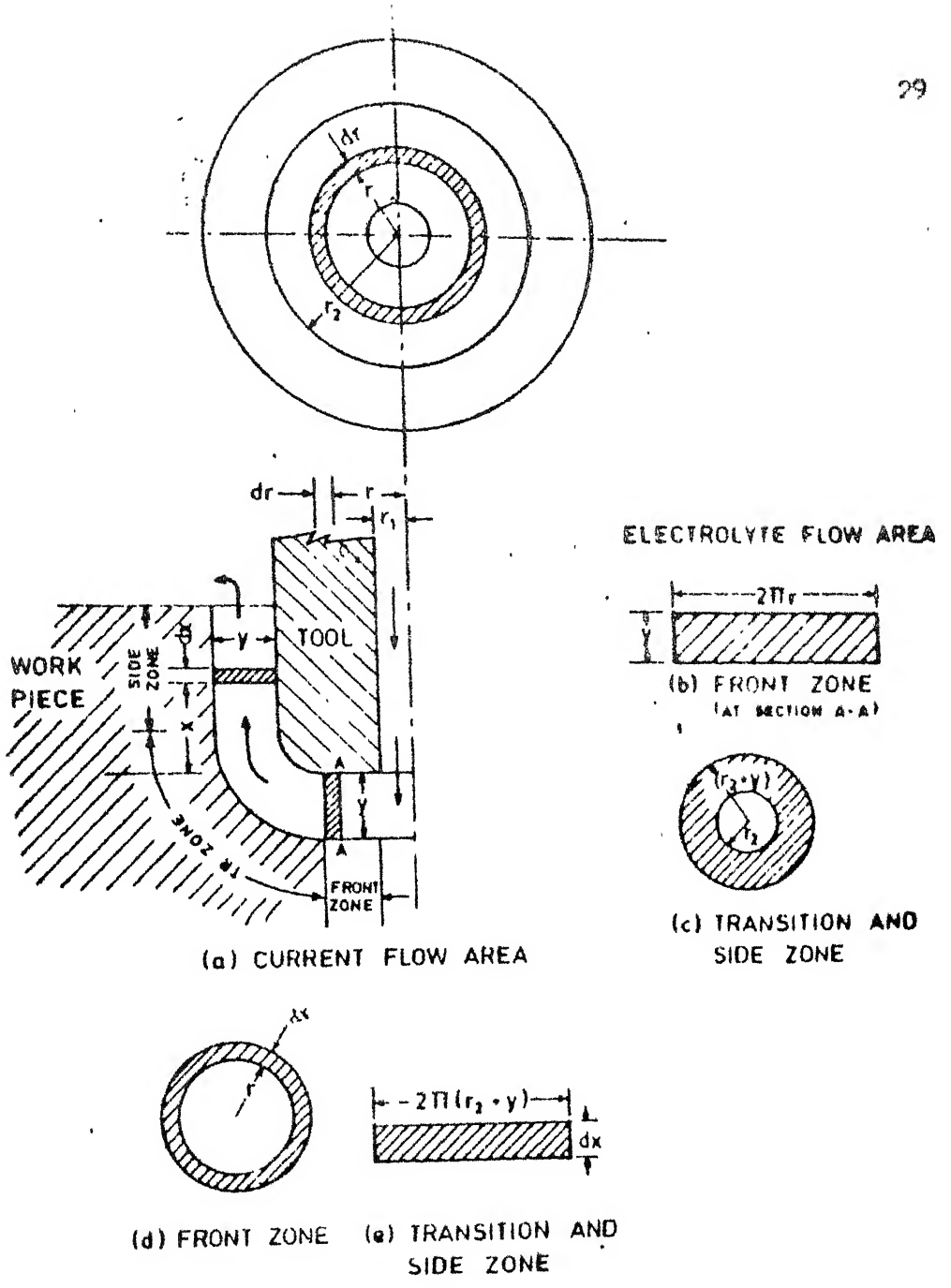

Fig.2.2 Electrolyte and current flow area for outward mode of electrolyte flow.

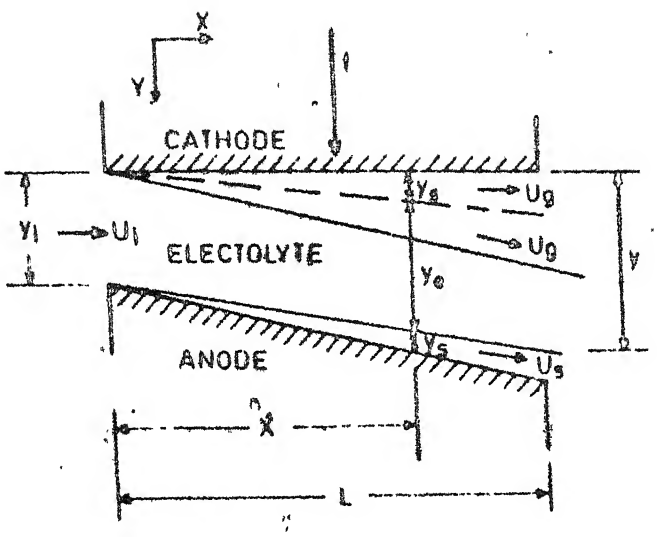

Fig. 2.3 Variation in gap width.

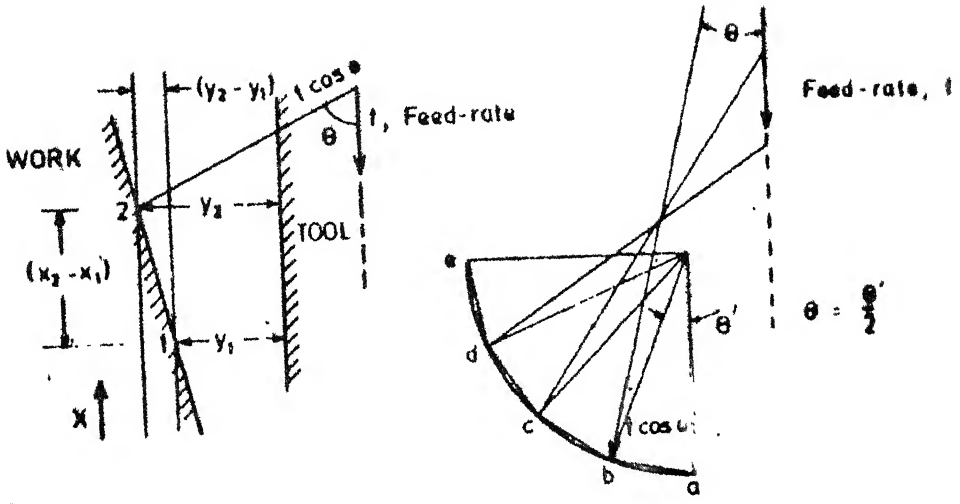

Fig. 2.4 Feed rate components in side and transition zones.

CHAPTER III

HEAT TRANSFER ANALYSIS OF ECM PROCESS — MODEL TFET22

3.1. INTRODUCTION

The aim of present day research in ECM is to devise an accurate and realistic methodology for tool-design. Conventional ECM tool-design is not accurate enough to account for heat transfer through the electrodes. Due to the complex nature of the process, in majority of the models for ECM tool-design, heat transferred from electrolyte to the electrodes has been neglected.

Tool materials generally employed during ECM are copper, brass, stainless steel, etc., which are good conductors of heat. Since large amount of heat is generated due to the Ohmic resistance of the electrolyte, considerable amount of heat will be transferred to the surroundings through electrodes. As the conductivity of the electrolyte, which is the most important machining parameter during ECM, is very sensitive to the temperature. Therefore heat transfer during ECM demands in-depth analysis.

Jain and Pandey [18] have suggested a simplified thermal resistance model for heat transfer analysis during ECM based on simplified assumptions like, unidirectional heat transfer, steady state heat transfer etc. It was concluded that the effect of heat transfer on the machining parameters during ECM is significant and ECM process must be analysed as a two or three dimensional heat transfer problem.

Here, an attempt has been made to analyse the heat transfer during EDM as two dimensional. Unsteady state, conjugate heat transfer problem. Finite element method has been applied for solving the governing differential equation.

3.2. CONJUGATE HEAT TRANSFER

When a solid material of finite dimensions and moderate conductivity is adjacent to a fluid flow domain, the temperature distribution in the fluid is coupled with the temperature field in the solid. Often, the thermal boundary condition is not prescribed at fluid-solid interface, but it is prescribed on the outer surface of the solid. This represents a conjugate heat transfer problem. If the conduction in the solid and the convection in the fluid were to be solved separately, then the matching procedure at the interface would have been very difficult. Here, the finite element method offers an easier alternative.

Since the finite element method can admit discontinuous conductivity distribution, all that is needed is to specify the solid conductivity to all the elements in solid region and fluid conductivity for all the elements in the fluid region. The solid-fluid interface will coincide with the control volume face, hence no boundary condition is needed there. The specified boundary condition at the outer surface of the solid can be directly used at the boundary the computational domain. The resulting solution will include the temperature distribution in the solid as well as the fluid.

In ECM process the electrolyte flows between tool and work (Figure 3.1). The heat transfer problem during ECM is a perfect conjugate heat transfer problem. The finite element discretization of the computational domain is shown in Figure 3.3. Once the governing differential equation is derived, the temperature distribution can be obtained by the finite element method.

3.3. FORMULATION OF THE PROBLEM

To derive the governing general differential equation, consider Figure 3.2 where energy balance analysis has been done for an elemental volume in the machining system as follows:

Energy in + Energy generated = Energy out

$$- K\Delta Y \frac{\partial T}{\partial x} - K\Delta X \frac{\partial T}{\partial Y} + \rho C_p U T \Delta Y + \dot{H}$$

$$- \rho C_p \Delta X \Delta Y \frac{\partial T}{\partial t} = - K\Delta X\left[\frac{\partial T}{\partial y} + \frac{\partial}{\partial y}\left(\frac{\partial T}{\partial y}\right)\Delta Y\right]$$

$$- K\Delta Y\left[\frac{\partial T}{\partial x} + \frac{\partial}{\partial x}\left(\frac{\partial T}{\partial x}\right)\Delta X\right]$$

$$+ \rho C_p \left(U + \frac{\partial U}{\partial x}\Delta X\right)\left(T + \frac{\partial T}{\partial x}\Delta X\right)\Delta Y$$

Simplification of about equation leads to

$$\rho C_p \frac{\partial T}{\partial t} = K\left[\frac{\partial^2 T}{\partial x^2} + \frac{\partial^2 T}{\partial y^2}\right] - \rho C_p U \frac{\partial T}{\partial x} + \dot{H} \qquad (3.1)$$

The above equation is derived assuming unidirectional fluid flow (x-direction only) and negligible heat generation due to viscous flow. To get the temperature distribution, it has to be solved subject to the boundary conditions as in Figure 3.3.

Equation (3.1) is fully applicable for an element in liquid zone. For an element in the solid region, the convection and heat generation terms will be zero.

3.4. FINITE ELEMENT ANALYSIS

The governing differential equation is,

$$K\left[\frac{\partial^2 T}{\partial x^2} + \frac{\partial^2 T}{\partial y^2}\right] - \rho C_p U \frac{\partial T}{\partial x} + \dot{H} - \rho C_p \frac{\partial T}{\partial t} = 0 \qquad (3.2)$$

With boundary conditions

(a) Temperature may be specified along the boundary

(b) It may be a convective boundary.

Let the temperature variation in the element be as follows:

$$T_e = a + bx + cy \qquad (3.3)$$

$$T_e = [N_1, N_2, \cdots] \begin{Bmatrix} T_1 \\ T_2 \\ \vdots \end{Bmatrix}$$

Then, the residue (R) is

$$R = K\left[\frac{\partial^2 T_e}{\partial x^2} + \frac{\partial^2 T_e}{\partial y^2}\right] - \rho C_p U \frac{\partial T_e}{\partial x} + \dot{H} - \rho C_p \frac{\partial T_e}{\partial t}$$

Galerkin method is used to minimize this residue,

$$\therefore \iint N_i R \, dx \, dy = 0$$

$$\text{or} \iint N_i \left[K\left(\frac{\partial^2 T_e}{\partial x^2} + \frac{\partial^2 T_e}{\partial y^2}\right) - \rho C_p U \frac{\partial T_e}{\partial x} + \dot{H} - \rho C_p \frac{\partial T_e}{\partial t}\right] dx \, dy = 0 \qquad (3.4)$$

First term of the eq. (3.4) is

$$\iint K N_i \frac{\partial^2 T_e}{\partial x^2} \, dx \, dy$$

Integrating with respect to x [24] gives

$$\iint K N_i \frac{\partial^2 T_e}{\partial x^2} \, dx \, dy = - \iint K N_{i,x} \frac{\partial T_e}{\partial x} \, dx \, dy + \int K N_{i,B} \frac{\partial T_e}{\partial x} n_x \, dB$$

where n_x is direction cosine along x-axis on the boundary of the domain.

Integrating the second term with respect to y gives

$$\iint K N_i \frac{\partial^2 T_e}{\partial y^2} \, dx \, dy = - \iint K N_{i,y} \frac{\partial T_e}{\partial y} \, dx \, dy + \int K N_{i,B} \frac{\partial T_e}{\partial y} n_y \, dB$$

where n_y is direction cosine along y-axis on the boundary of the domain.

$$\therefore \iint K \left[\frac{\partial^2 T_e}{\partial x^2} + \frac{\partial^2 T_e}{\partial y^2} \right] dx \, dy = - \iint K \left[N_{,x} \frac{\partial T_e}{\partial x} + N_{,y} \frac{\partial T_e}{\partial y} \right] dx \, dy + \int N_{iB} \left[K \frac{\partial T_e}{\partial x} n_x + K \frac{\partial T_e}{\partial y} n_y \right] dB$$

$$= \iint K \left[N_x \frac{\partial T_e}{\partial x} + N_y \frac{\partial T_e}{\partial y} \right] dx \, dy - \int q \, N_{i,B} \, dB$$

$$= \iint K \left[\{N_x\} \lfloor N_x \rfloor + \{N_y\} \lfloor N_y \rfloor \right] dx \, dy \{T\} - \int h(T - T_o) N_{i,B} \, dB$$

$$= - [K_s] \{T\} - h \int \{N_B\} \lfloor N \rfloor \{T\} \, dB + h \, T_o \int N_B \, dB$$

$$= - [K_s] \{T\} - [B1] \{T\} + [B2] \qquad (3.5)$$

Third term is,

$$- \int\int \rho C_p U \frac{\partial T}{\partial x} N_i \, dx \, dy$$

$$= - \int\int \rho C_p U \{N\} [N_x] \, dx \, dy \, \{T\}$$

$$= - [A] \{T\}$$

Fourth term is,

$$\int\int N_i \dot{H} \, dx \, dy$$

$$= \dot{H} \int\int \{N_i\} \, dx \, dy = P$$

Fifth term is,

$$- \int\int \rho C_p \frac{\partial T_e}{\partial t} N_i \, dx \, dy$$

$$= - \int\int \rho C_p \{N\} [N] \, dx \, dy \{\dot{T}\} = -[M] \{\dot{T}\}$$

Finally by combining,

$$- [K_s] \{T\} - [B1] \{T\} + [B2] - [A] \{T\} + \{P\} - [M] \{\dot{T}\} = 0$$

or

$$[[K_s] + [B_1] + [A]] \{T\} + [M] \{\dot{T}\} = \{P\} + \{B2\}$$

Let $[D] = [K_s] + [B1] + [A]$

and $[B] = \{P\} + \{B2\}$

Then

$$[M] \{\dot{T}\} + [D] \{T\} = \{B\} \qquad (3.6)$$

3.4.1. GENERATION OF DIFFERENT MATRICES FOR TRIANGULAR ELEMENTS

For triangular elements (Figure 3.4(a)), the temperature is assumed to vary as

$$T = a + bx + cy = [N]\{T\}$$

Let

$$b_1 = Y_2 - Y_3$$
$$b_2 = Y_3 - Y_1$$
$$b_3 = Y_1 - Y_2$$
$$c_1 = X_3 - X_2$$
$$c_2 = X_1 - X_3$$
$$c_3 = X_2 - X_1$$

Area of the element is given by,

$$\Delta = \frac{1}{2}\left[x_1(y_2 - y_3) + x_2(y_3 - y_1) + x_3(y_1 - y_2)\right]$$

Interpolating functions are given by,

$$N_1 = \frac{1}{2\Delta}\left[xy_2 - x_2y + x_2y_3 - x_3y_2 + x_3y - xy_3\right]$$

$$N_2 = \frac{1}{2\Delta}\left[x_1y - xy_1 + xy_3 - x_3y + x_3y_1 - x_1y_3\right]$$

$$N_3 = \frac{1}{2\Delta}\left[x_1y_2 - x_2y_1 + x_2y - xy_2 + xy_1 - x_1y\right]$$

$$N_{,x} = \frac{1}{2\Delta}\left[b_1 \quad b_2 \quad b_3\right]$$

$$N_{,y} = \frac{1}{2\Delta}\left[c_1 \quad c_2 \quad c_3\right]$$

The matrix $[K_s]$ is

$$[K_s] = K \int\int \left[\{N_x\}[N_x] + \{N_y\}[N_y]\right] dx\, dy$$

$$= \frac{K}{4A} \begin{matrix} b_1^2 + c_1^2 & b_1b_2 + c_1c_2 & b_1b_3 + c_1c_3 \\ & b_2^2 + c_2^2 & b_2b_3 + c_2c_3 \\ \text{Sym} & & b_3^2 + c_3^2 \end{matrix}$$

$$[A] = \rho C_p U \int [N] [N_x] \, dx \, dy$$

$$= \frac{\rho C_p U}{6} \begin{matrix} b_1 & b_2 & b_3 \\ b_1 & b_2 & b_3 \\ b_1 & b_2 & b_3 \end{matrix}$$

$$[P] = \dot{q} \int [N] \, dx \, dy$$

$$= \frac{\dot{H}A}{3} \begin{Bmatrix} 1 \\ 1 \\ 1 \end{Bmatrix}$$

3.3.2. BOUNDARY MATRICES

The boundary matrices are:

$$[B1] = h \int_B [N] [N] \, dB$$

$$[B2] = h T_o \int_B [N] \, dB$$

Thus for evaluating these convective boundary matrices, the convective boundary B must be known. If the edge i,j is along the convective boundary (Figure 3.4(a)), then,

$$[B1] = \frac{h.S_{ij}}{6} \begin{bmatrix} 2 & 1 & 0 \\ 1 & 2 & 0 \\ 0 & 0 & 0 \end{bmatrix}$$

$$B2_{ij} = \frac{h.T_o.S_{ij}}{2} \begin{Bmatrix} 1 \\ 1 \\ 0 \end{Bmatrix}$$

If the edge jk of the element is along the convective boundary, then

$$B1_{jk} = \frac{h.S_{jk}}{6} \begin{bmatrix} 0 & 0 & 0 \\ 0 & 2 & 1 \\ 0 & 1 & 2 \end{bmatrix}$$

$$B2_{jk} = \frac{h.T_o.S_{jk}}{2} \begin{Bmatrix} 0 \\ 1 \\ 1 \end{Bmatrix}$$

If ki is along the boundary, then

$$B1_{ki} = \frac{h.S_{ki}}{6} \begin{bmatrix} 2 & 0 & 1 \\ 0 & 0 & 0 \\ 1 & 0 & 2 \end{bmatrix}$$

$$B2_{ki} = \frac{h.T_o.S_{ki}}{2} \begin{Bmatrix} 1 \\ 0 \\ 1 \end{Bmatrix}$$

3.5. METHOD USED FOR SOLVING THE SYSTEM OF LINEAR DIFFERENTIAL EQUATIONS

In order to get the temperature distribution, the system of linear differential equations given by eq. (3.6) has to be solved. The following method is adopted for that purpose.

$$[M]\{\dot{T}\} + [D]\{T\} = \{B\} \qquad (3.6)$$

From the Figure 3.4(b) $\dot{T}$ is given by

$$\dot{T} = T^{k+1} - \theta \frac{T}{t}^{k+1} \Delta t \quad \text{(Backward integration)}$$

$$= T^{k} + (1 - \theta) \frac{T}{t}^{k} \Delta t \quad \text{(Forward integration)}$$

where

θ is a fraction $0 \quad \theta \quad 1$

and Δt is time interval

$$[M]\{T\}^{k+1} - \theta(\dot{T})^{k+1} \Delta t = [M]\{T\}^{k} + (1 - \theta)\dot{T}^{k} \Delta t \tag{3.7}$$

From eq. (3.6)

$$[M]\{\dot{T}\}^{k+1} + [D]\{T\}^{k+1} = \{B\}^{k+1} \tag{3.8}$$

$$[M]\{\dot{T}\}^{k} + [D]\{T\}^{k} = \{B\}^{k} \tag{3.9}$$

Using eqs. (3.8) and (3.9) in eq. (3.6)

$$[K]\{T\}^{k+1} + \theta \Delta t \left[[D]\{T\}^{k+1} - \{B\}^{k+1}\right]$$

$$= [M]\{T\}^{k} + (1 - \theta)\Delta t \left[\{B\}^{k} - [D]\{T\}^{k}\right]$$

For $\{B\}^{k+1} = \{B\}^{k}$

$$\left[[M] + \theta \Delta t [D]\right]\{T\}^{k+1} = \left[[M] - (1 - \theta)\Delta t [D]\right]\{T\}^{k} + \left[(1 - \theta)\Delta t\{B\} + \theta \Delta t\{B\}\right]$$

For $\theta = 1$ (Backward integration)

$$\left[[M] + \Delta t [D]\right]\{T\}^{k+1} = [M]\{T\}^{k} + \Delta t\{B\}^{k}$$

Dividing by Δt

$$\left[\frac{1}{\Delta t}[M] + [D]\right]\{T\}^{k+1} = \frac{1}{\Delta t}[M]\{T\}^{k} + \{B\}^{k} \tag{3.10}$$

Now the problem is simplified. To get the temperature distribution, the system of linear equations given by eq. (3.10) has to be solved.

3.6. RESULTS AND DISCUSSION

Electrochemical machining experiments with plane parallel electrodes were conducted by Bhatia [21, 22] using copper, brass and stainless steel as tool materials, mild steel as work material and NaCl solution in water as electrolyte. Temperature at distances as 2.5, 6.5, 17.5 and 21.5 mm from one end were measured using thermocouples. The experimental conditions and temperature data are given in Table 2. Murugan [11] conducted one dimensional heat transfer analysis of ECM process using thermal resistance model [18]. He tested his model using experimental data reported in reference [8]. In this analysis, heat transferred by conduction mode alone was considered, and heat transfer by convection was neglected. As a result of such simplified assumptions a discrepancy (Figure 3.6) is observed between analytical and experimental results. Keeping this in view, the problem has been analysed as a two dimensional, single phase transient heat transfer problem.

Figure 3.6 shows the comparison of experimental results, one dimensional heat transfer results and the results obtained by the present model for different tool materials. Results have also been plotted (Figure 3.5) for the case, when heat transfer through the electrodes is neglected (Model FET22). It can be seen from the figures that the results obtained by the present model are closer to the experimental data. This clearly shows

the importance of incorporating two dimensional, transient heat transfer in ECM analysis. However, the discrepancy between experimental and analytical results can be further reduced by analysing the problem as a three dimensional multiphase transient heat transfer problem.

Figure 3.5 shows the temperature distribution along both the tool and workpiece. It can be seen that, for stainless steel material, the temperatures along the tool and workpiece are almost equal. But for copper as tool material some difference is observed between the temperatures along the work and tool. This is mainly because of different thermal conductivities of work and tool materials.

However, comparatively large discrepancies between the analytical and experimental results (Figure 3.6(d)) are exhibited at the inlet side for the case of copper as tool material. However, the deviation in case of present model is less when compared to one dimensional heat transfer analysis. This is because of the fact that there will be some transfer of heat from exit to inlet side due to temperature gradient.

The discrepancy between analytical and experimental results can be attributed to the following reasons. Effect of void fraction has not been considered in this model. Exact values of valency of dissolution and machining efficiency are not known. The sources of heat, other than Ohmic heating have also been neglected.

3.7. CONCLUSIONS

From results and discussion, following conclusions have been drawn:

(1) The two dimensional, transient heat transfer model yields results that are closer to the experimental data when compared to the results obtained by thermal resistance model or one dimensional FE model.

(2) Cathode material has significant effect on temperature distribution along the electrolyte flow path. Consequently it would have an effect on machined profile of the component.

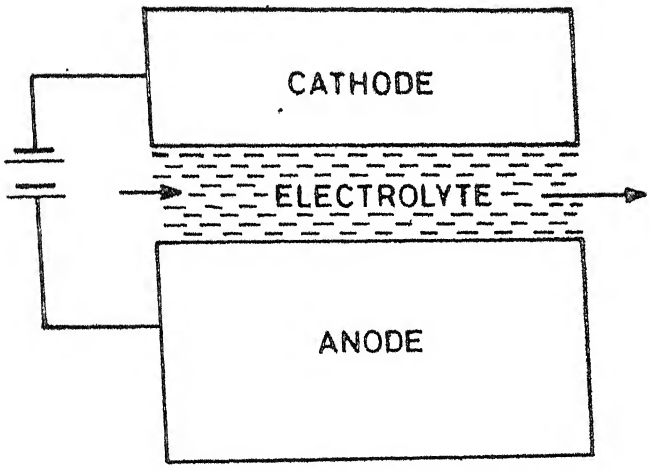

FIG. 3.1 SCHEMATIC DIAGRAM OF ECM PROCESS.

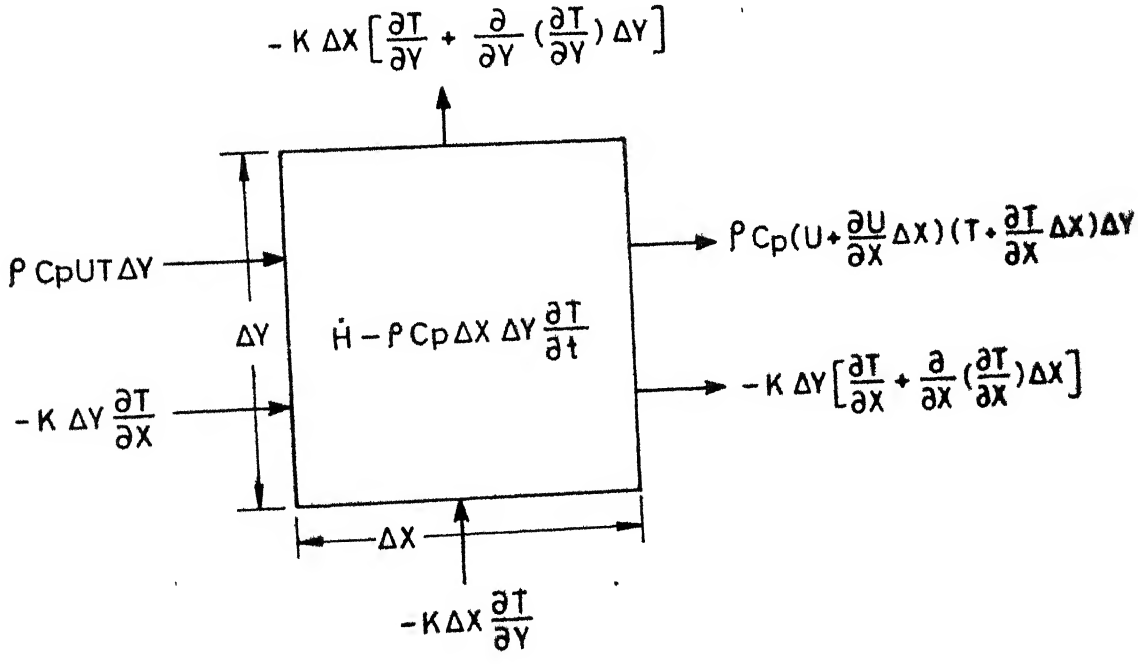

FIG. 3.2 CONTROL VOLUME FOR ENERGY ANALYSIS.

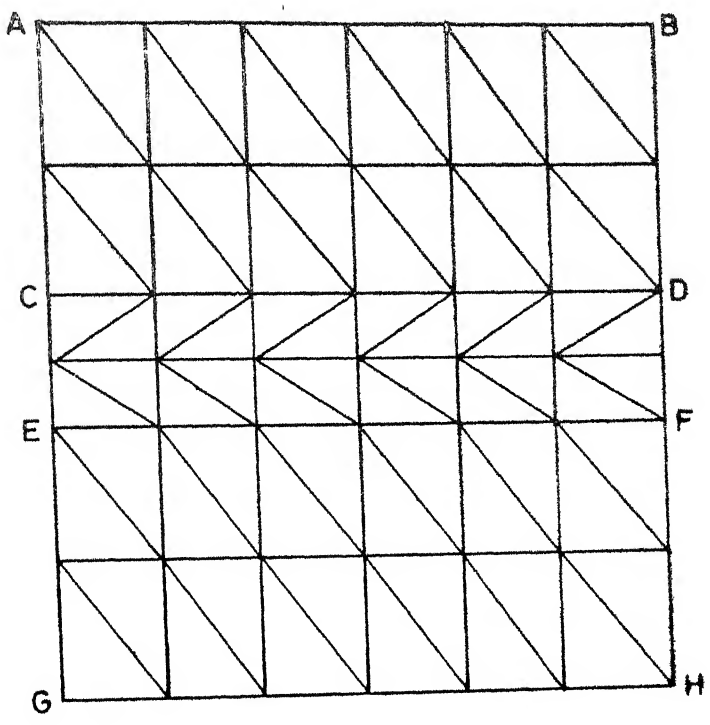

BOUNDARY	CONDITION
AC, BD	CONVECTIVE
EG, FH	CONVECTIVE
AB, GH	INSULATED $(\frac{\partial T}{\partial Y} = 0)$
CE	TEMPERATURE SPECIFIED $(T = T_o)$
DF	INSULATED $(\frac{\partial T}{\partial X} = 0)$

FIG. 3.3 FINITE ELEMENT DISCRETIZATION OF ECM SYSTEM.

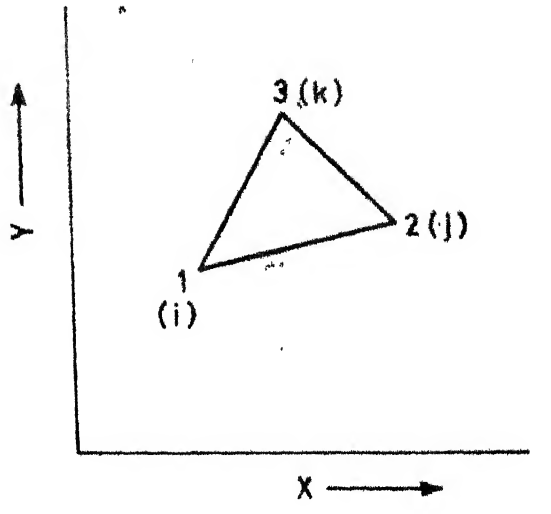

(a)

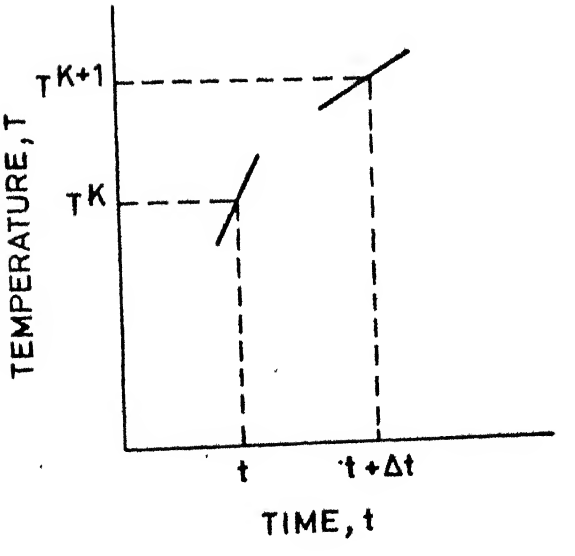

(b)

FIG. 3.4 TYPICAL TRIANGULAR ELEMENT.

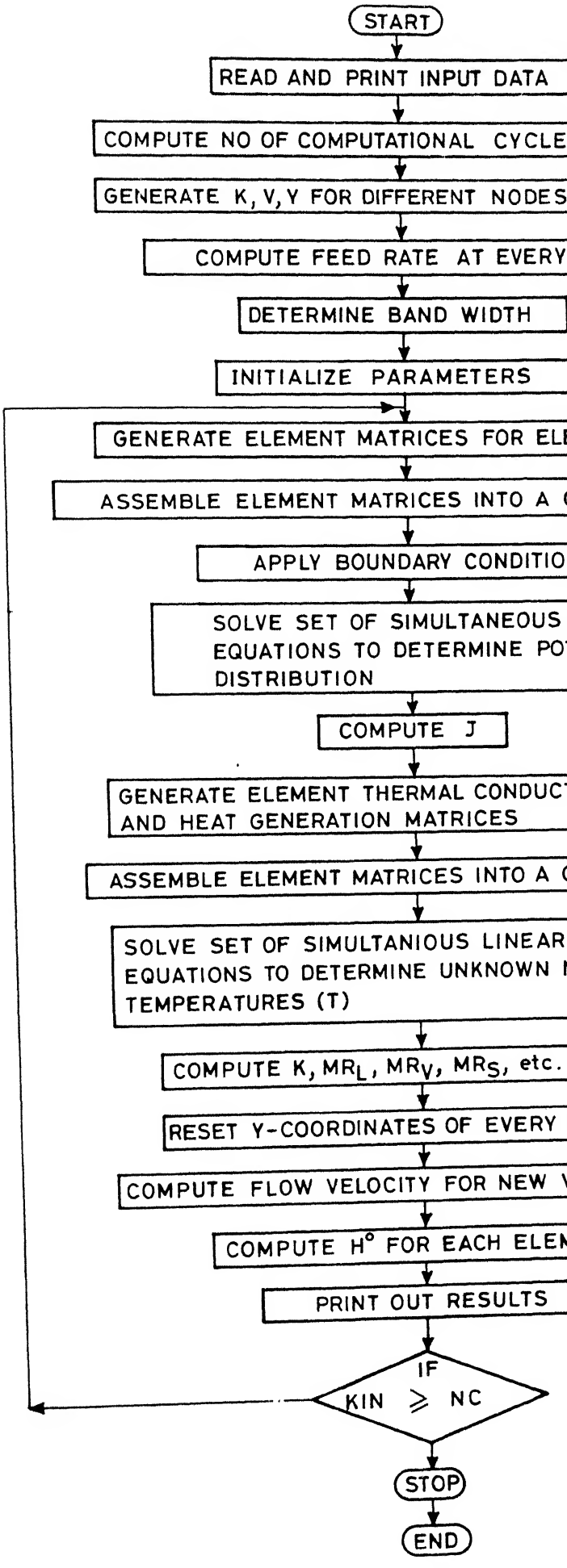

FIG. 3.4(c) FLOW CHART FOR MODEL TFET-22.

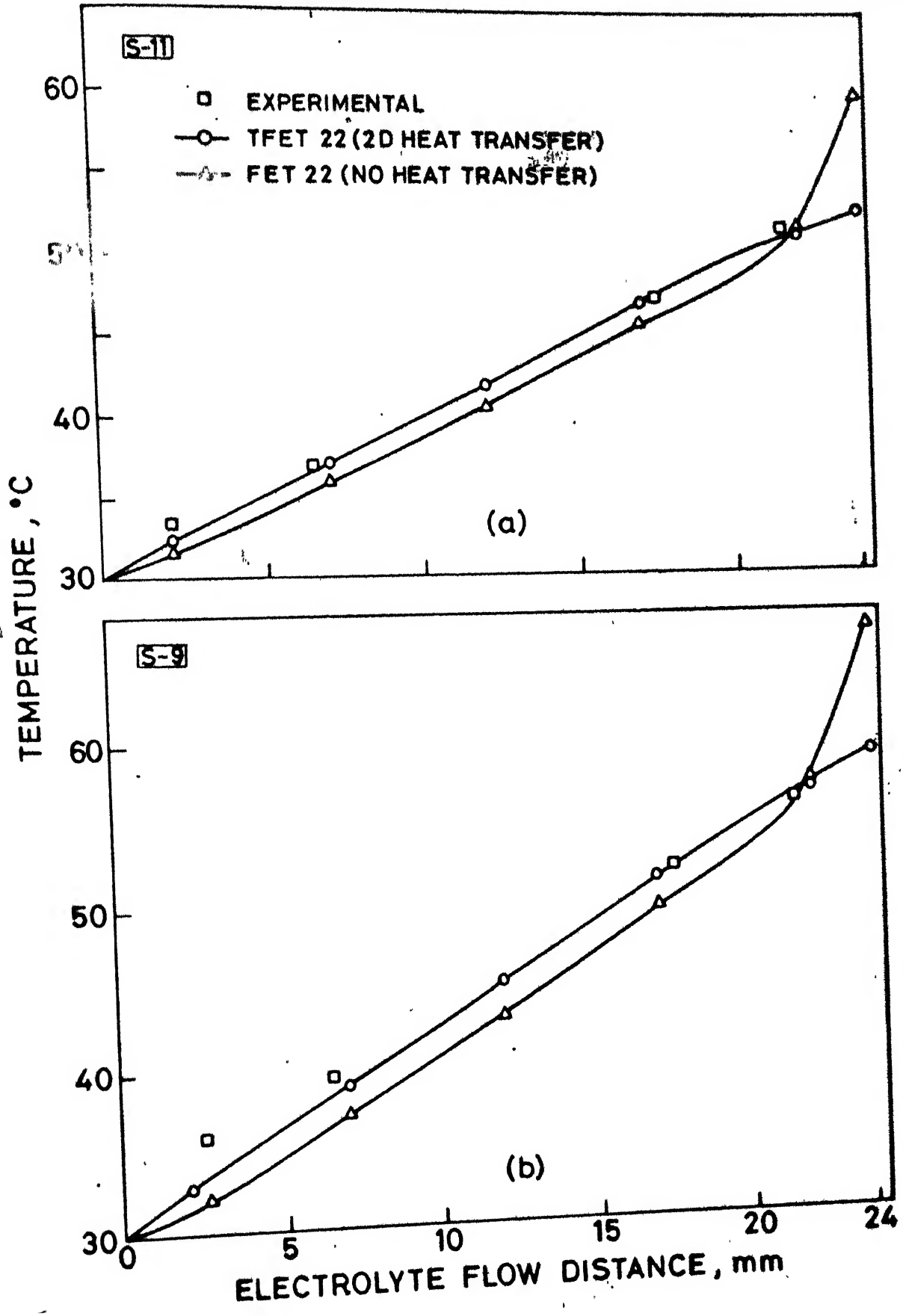
S-11
EXPERIMENTAL
TFET 22 (2D HEAT TRANSFER)
FET 22 (NO HEAT TRANSFER)
60
40
30
(a)
S-9
60
50
40
30
(b)
0
5
10
15
20
24
TEMPERATURE, °C
ELECTROLYTE FLOW DISTANCE, mm

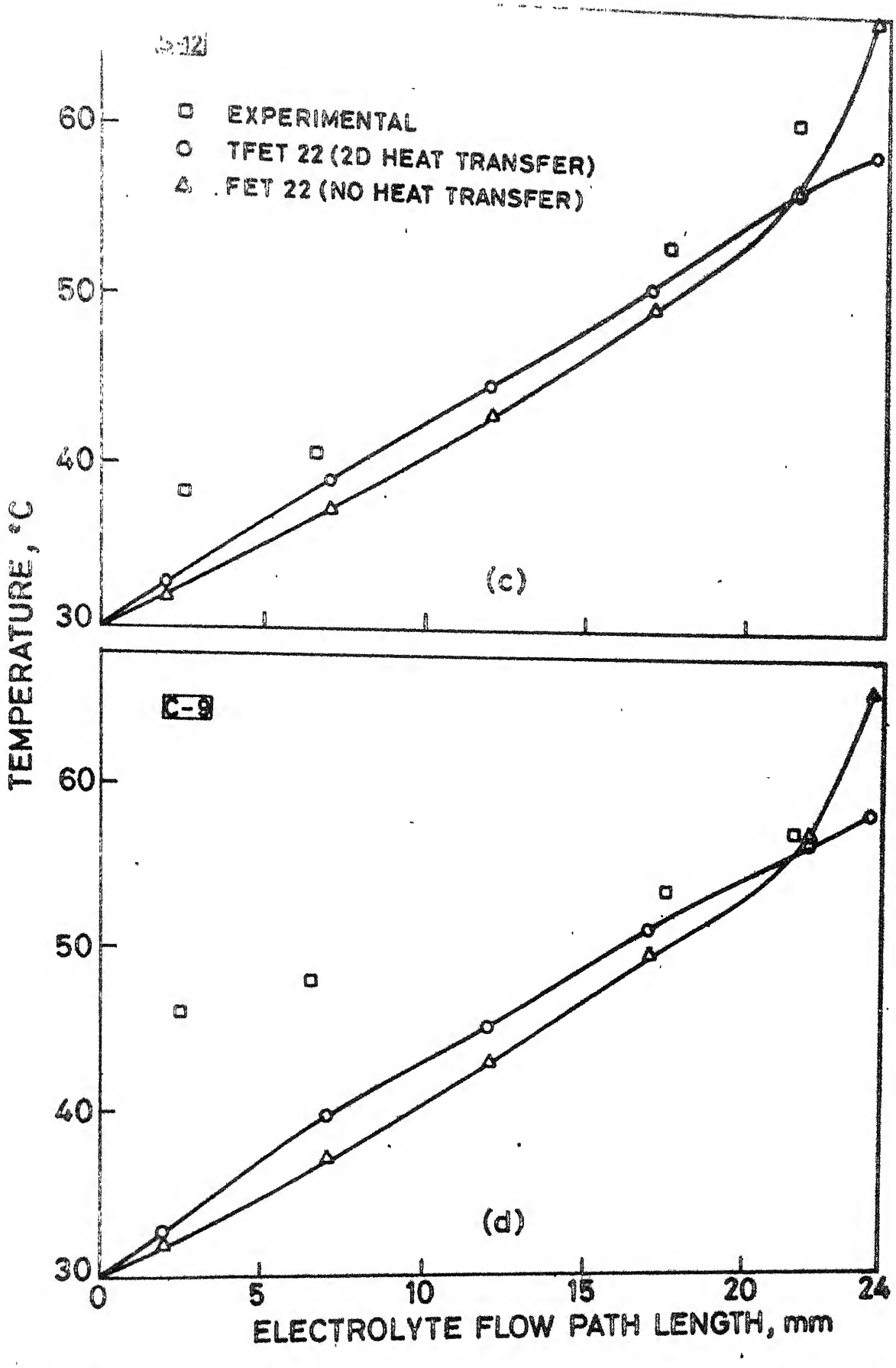

FIG. 3.5 COMPARISON OF EXPERIMENTAL AND ANALYTICL TEMPERATURE DISTRIBUTION.

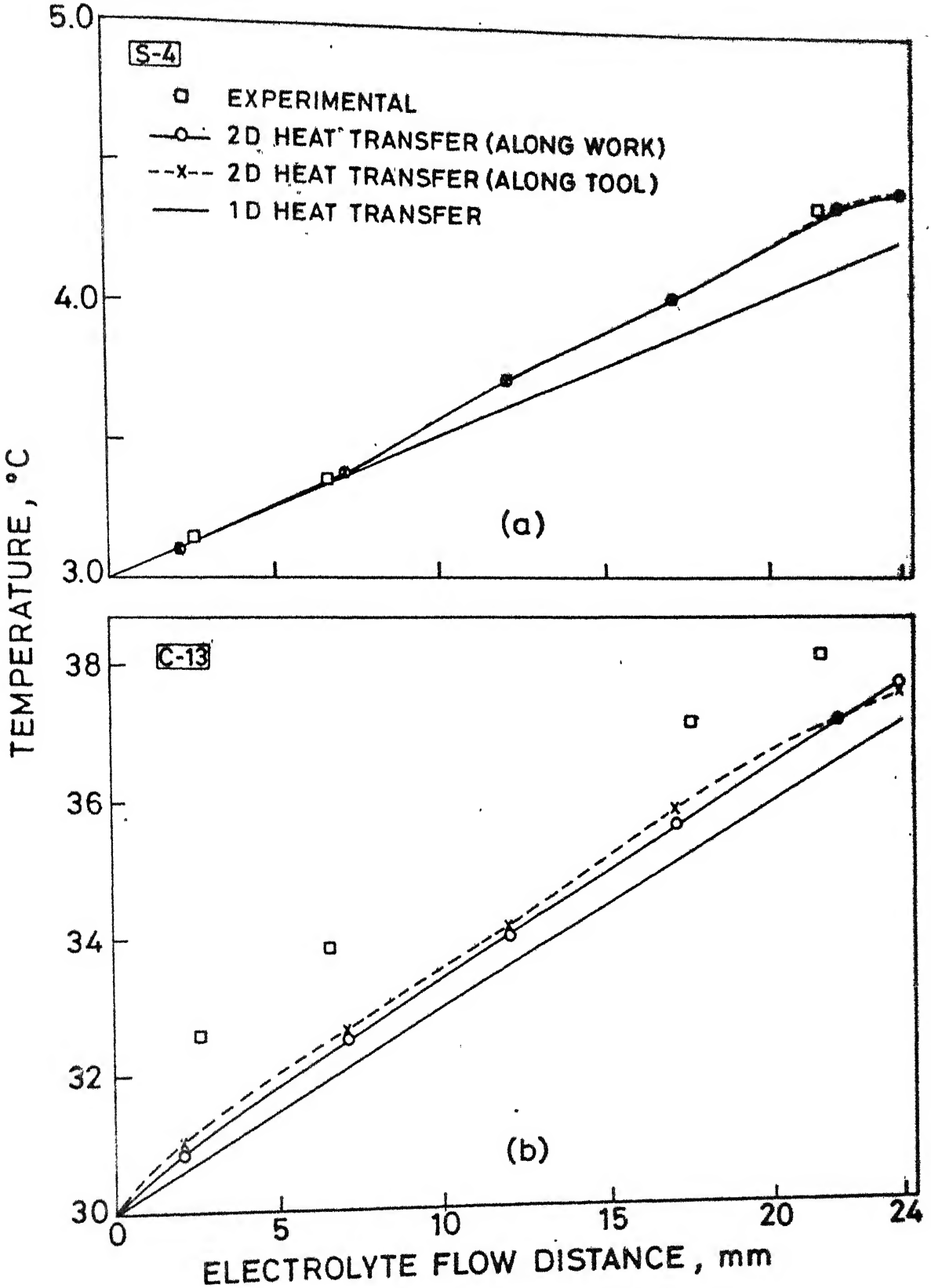
S-4
EXPERIMENTAL
2D HEAT TRANSFER (ALONG WORK)
2D HEAT TRANSFER (ALONG TOOL)
1D HEAT TRANSFER
(a)
C-13
(b)
TEMPERATURE, °C
ELECTROLYTE FLOW DISTANCE, mm
5.0
4.0
3.0
38
36
34
32
30
0
5
10
15
20
24

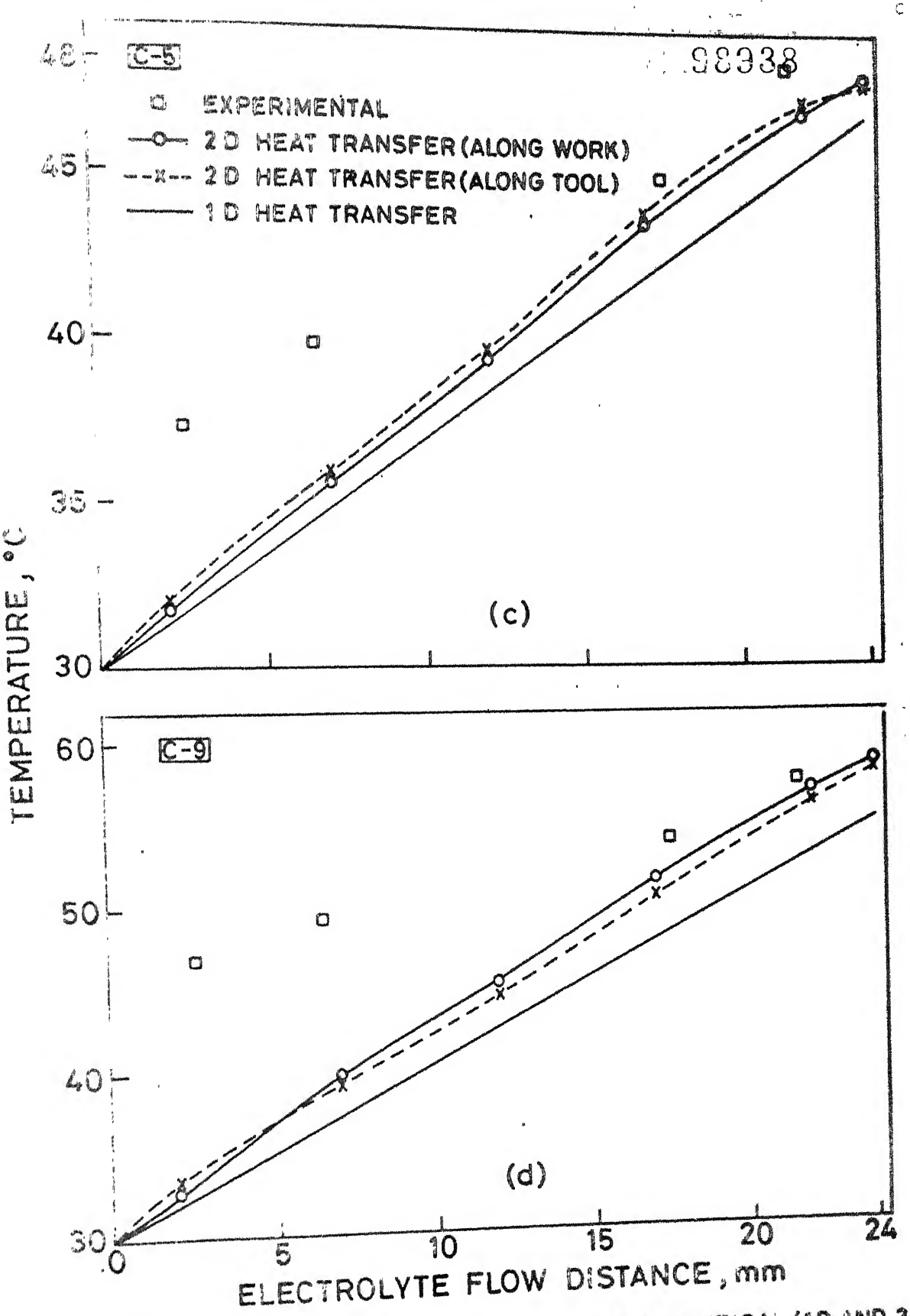

FIG. 3.6 COMPARISON OF EXPERIMENTAL AND ANALYTICAL (1D AND 2D HEAT TRANSFER) TEMPERATURE DISTRIBUTIONS.

CHAPTER IV

TOOL DESIGN

4.1. INTRODUCTION

The most important aspect in the design of ECM tools is the prediction of tool shape to produce the specified workpiece shape. It is well known that, tool shape is not simply the workpiece shape reduced (or increased) by some machining gap dimensions. The gap is not constant over the machining surface. It is a function of different machining parameters.

Due to complex nature of ECM process, majority of the models proposed for ECM tool design, do not account for the variations in the process parameters such as temperature, void fraction, etc. For an accurate tool design in ECM, variations in all the process parameters and their effects on anode profile should be considered.

'Correction Factor Method' has been suggested by Reddy [26] for the purpose of tool design in ECM. In this chapter, a two dimensional model for predicting a cathode configuration which can produce specified anode shape under prescribed machining conditions has been described. Cathode shape design problem has been attempted for different cases viz., ECD, ECBD and ECB. Anode shape prediction model, developed by Jain and Yogindra [12] has been used for ECD and ECBD. This model has been modified for the prediction of work shape with a tapered tool. This model has been used in the tool design package. It has also been modified for the prediction of anode shape in ECB.

4.2. GENERAL DESIGN PROCEDURE

Tool design procedure for producing the required work shape while machining under given conditions is summarized as follows.

INITIAL TOOL SHAPE

The first step is to assume a tool shape depending on the required work shape and type of ECM operation e.g. ECD, ECDD, ECB etc. For most of the cases, the tool shape can be assumed as congruent to the desired work shape.

WORK SHAPE PREDICTION

The second step is to predict the work shape obtainable from the assumed tool shape. There are many models available for anode shape prediction in ECM. The models based on numerical methods like FEM, can predict work profiles within a reasonable accuracy.

ERROR AND CORRECTION

The third step is to compare the predicted work shape with the required work shape and to obtain deviations between them. If the deviation is more than the specified tolerance, correction required to minimize this error has to be calculated.

MODIFICATION

The fourth step is to modify the present tool shape by applying the correction appropriately. Using this modified tool, again the anode shape is predicted. Steps 2, 3 and 4 are

repeated till the work shape within the desired tolerance is obtained (see Figure 4.4(d)). This procedure consists of a number of design cycles. Tool is refined progressively in each design cycle. Finally it gives the tool shape whhh will produce desired work shape.

From the above procedure, it is clearly evident that the soul of this method is anode shape prediction model. Any inaccuracy associated with anode shape prediction model will be reflected on the designed tool shape.

4.3. ELECTROCHEMICAL DRILLING

Here, an attempt has been made to design,

(1) Bare tool for electrochemical drilling

(2) Tool bit for electrochemical bit drilling (ECBD).

4.3.1. INITIAL TOOL SHAPE

Initial tool shape has been assumed as cylindrical one, having a radius equal to 1 mm lesser than the required hole radius at the end of transition zone. In case of transition zone, tool corner radius has been assumed again as 1 mm lesser than the required work corner radius.

4.3.2. PREDICTION OF ANODE SHAPE

In the anode shape prediction model, the field distribution is obtained by solving the Laplace equation $\left(\frac{\partial^2 \phi}{\partial x^2} + \frac{\partial^2 \phi}{\partial y^2} = 0\right)$ with the following boundary conditions,

(a) $\phi = 0$ along cathode (tool)

(b) $\phi = V - \Delta V$ along anode (work)

(c) $\frac{\partial \phi}{\partial n} = 0$ along open edges.

Since ECD is a moving boundary problem, the domain length and width will change after each computational machining cycle time, Δt sec. As the tool penetrates in the work surface, the total number of nodes would also increase. The coordinates of each node, therefore should be adjusted. Figure 4.2 shows renumbering of nodes after one cycle of computational machining. In Δt sec., tool penetrates to a depth equal to the length of an element which is assumed to be same in all zones. Here, an assumption has been made that the feed to the tool is given only after machining has taken place for a time interval of Δt sec., i.e., the process is considered like intermittent cutting rather than continuous one, as in actual ECM.

The IEG's in the beginning of a computational machining cycle will get modified in the following cycle. Also, the tool will occupy new position after a computation machining cycle (Figure 4.3). The modified IEG's are assigned to the corresponding points on the tool in new position, in order to obtain work shape at the end of that computational machining cycle (Figure 4.3).

4.3.3. CALCULATION OF ERROR AND CORRECTION

The coordinate system for all the three zones viz., front, transition and side zones, is shown in Figure 4.1. The coordinate system is selected in such a way that the error calculation principle remains the same for all the three zones. The error and correction at each node are calculated as follows:

$$\text{ERROR}(I) = \text{OWS}(I) - \text{RWS}(I) \qquad (4.1)$$

$$\text{CORR}(I) = -\text{ERROR}(I) \qquad (4.2)$$

where

CORR(I) = Correction to be made at Ith node

OWS(I) = Y coordinate of the obtained work shape at Ith node

RWS(I) = Y coordinate of the required work shape at Ith node.

The correction need not always be equal to error in all the design cycles. It can be calculated from the trend of the past design cycle. This may some times give less CPU time. From the second design cycle onwards, the correction can be calculated as given below:

$$CORR_k(I) = \frac{CORR_{k-1}(I) \times ERROR_k(I)}{ERROR_{k-1}(I) - ERROR_k(I)} \qquad (4.3)$$

where suffix k stands for the present design cycle and suffix k-1 stands for the previous design cycle.

Equation (4.3) gives the correction that has to be applied ($CORR_k(I)$) for minimizing the present error ($ERROR_k(I)$). In the present work eq. (4.2) has been used.

4.3.4. MODIFICATION

The tool used in the previous design cycle is modified by applying correction to the Y coordinates of the tool at different nodes. However, in the side zone, the correction should be applied in normal direction to the work profile at that node, since the machining takes place in that direction (Figure A.2, Appendix-I). But in the anode shape prediction model, IEG's are considered to be perpendicular to the axis of

the tool. Correction is also applied along the same direction, in order to obtain new tool shape.

$$NIS(I) = Y(I) + CORR(I) \qquad (4.4)$$

where NTS(I) = Y coordinate of the new tool shape at Ith node

Y(I) = Y coordinate of tool in previous cycle.

Correction at any node (CORR(I)) may be positive or negative depending on the deviation between the ontained work shape and required work shape at that node.

In ECD, unlike plane parallel electrodes ECM, as the machining progresses, a node on workpiece is exposed to different nodes on the tool at different times. This makes designing more difficult in ECD with bare tool. If the tool shape at a node is changed, that it will affect the work shape at many nodes, on its way. Later problem is eliminated, to some extent, in case of ECBD.

4.4. TOOL BIT DESIGN FOR ECBD

Beyond the bit height region, sides of the drilled hole or predicted hole, during ECBD, will be reasonably straight. In the bit height region, it will be tapered. Tool bits can be designed to produce straight sided through holes with a reasonably good accuracy. Initial bit shape is assumed to be 1 mm smaller in diameter than the required work shape. The designing procedure is on similar lines as discussed above. Only difference is in the anode shape prediction model, that is the nodes beyond the bare bit height will remain inactive.

treated in the same way as in ECD. The other details have been given in Appendix-I.

4.5.2. TOOL BIT DESIGN FOR ECBB

Tool bits have been designed to enlarge and correct the predrilled hole. The initial tool bit is assumed to be 1 mm smaller than the desired hole. The designing procedure is on same lines as in ECBD. The other details have been discussed in Appendix-I.

4.6. RESULTS AND DISCUSSION

Jain [8] conducted experiments (Tables 3 and 4) using brass as material for tool and low alloy steel castings and low alloy steel forgings as materials for anode. The shape and size of the profiles were measured by preparing a cast replica of the hole and projecting it on a tool maker's microscope. The method by which anode corner radius was measured, has been described in detail in [8]. Tools have been designed for producing profiles obtained experimentally. The designed tool shapes have been compared with these experimental tools (Figures 4.5 and 4.8).

4.6.1. ELECTROCHEMICAL DRILLING

Figure 4.5 shows a comparison between the designed tool shape and the tool shape used during experimentation for the case of ECD with bare tool. Here, the required and obtained work shapes are coinciding because, the design procedure is continued till the deviation between the required and obtained work shapes lie within an accuracy of 5 μm.

Kinks, just opposite to the unevenness in the experimental work profile, are observed in the designed tool shape. This is mostly observed at the end of the transition zone and near the top surface of the drilled hole. Kinks obtained during designing of the top of the tool (Figure 4.5(b)) is mainly because of the curved surface at the top of the work surface produced due to stray current attack.

Figure 4.6 shows the designed bare tool for producing a straight sided hole during ECD. It is important to note that the designed tool shape may not produce the straight sided hole with the specified accuracy, because of the following reason.

The stray current attack on the work surface is more with the bare tools when compared to bit type or coated tools. But in the anode shape prediction model, there is no provision to account for the stray current attack.

4.6.2. ELECTROCHEMICAL BIT DRILLING

Figure 4.7 shows the designed tool bit for producing a straight sided hole. The design is based on the assumption that the voltage remains constant throughout the machining. In other words, the designed tool shape will produce a straight hole only when, voltage fluctuations during the machining are arrested.

Figure 4.8 shows a comparison of designed tool bit and the one used during experimentation for the case of electrochemical bit drilling. Difference can be observed between the obtained and required work shapes at the top of the drilled hole (Figure 4.8 (a & b)). This is again, because of the same reason that the stray current attack is not considered in anode shape prediction model.

4.6.3. ELECTROCHEMICAL BIT BORING

Figure 4.9 shows the designed tool bit for enlarging and straightening the predrilled hole in case of ECBB. As the experimental data are not available, the comparison between the designed and experimental tools is not made.

4.6.4. GENERAL DISCUSSION

The discrepancy between the designed tool profile and the tool profile used during experimentation is attributed to the following reasons:

(1) The main reason is the inaccuracy of anode shape prediction model.

(2) The discrepancy in the transition zone is mainly due to the inaccurate measurement of overcut in this zone. The overcut at the end of transition zone was measured by replica technique. Taking overcut at the end of transition zone as radius, an arc was drawn in the whole transition zone, assuming that the overcut in transition zone remains constant. But in actual practice, the IEG at the beginning of the transition zone is normally smaller than that at the end of transition zone.

As discussed earlier, the accuracy of the tool design model mainly depends on the accuracy of anode shape prediction model. The factors responsible for the poor accuracy of the anode shape prediction model (SBFET22) are as follows:

(1) Stray current attack is not considered.

(2) Electrolyte flow velocity distribution in IEG is obtained from the continuity equation alone.

(3) Correct values of valency of EC dissolution, machining efficiency, accurate electrochemical equivalent of alloys and behaviour of gas bubbles distribution in IEG etc. are not known.

4.7. CONCLUSIONS

There is a good agreement between the designed tool shape and the experimental tool shape for the same machining conditions. However, the accuracy of the proposed correction method for tool design in ECM, depends mainly on the accuracy of anode shape prediction model. The designed tool shape is not the complementary shape of the desired work shape in all the cases, i.e., ECD, ECBD and ECBB.

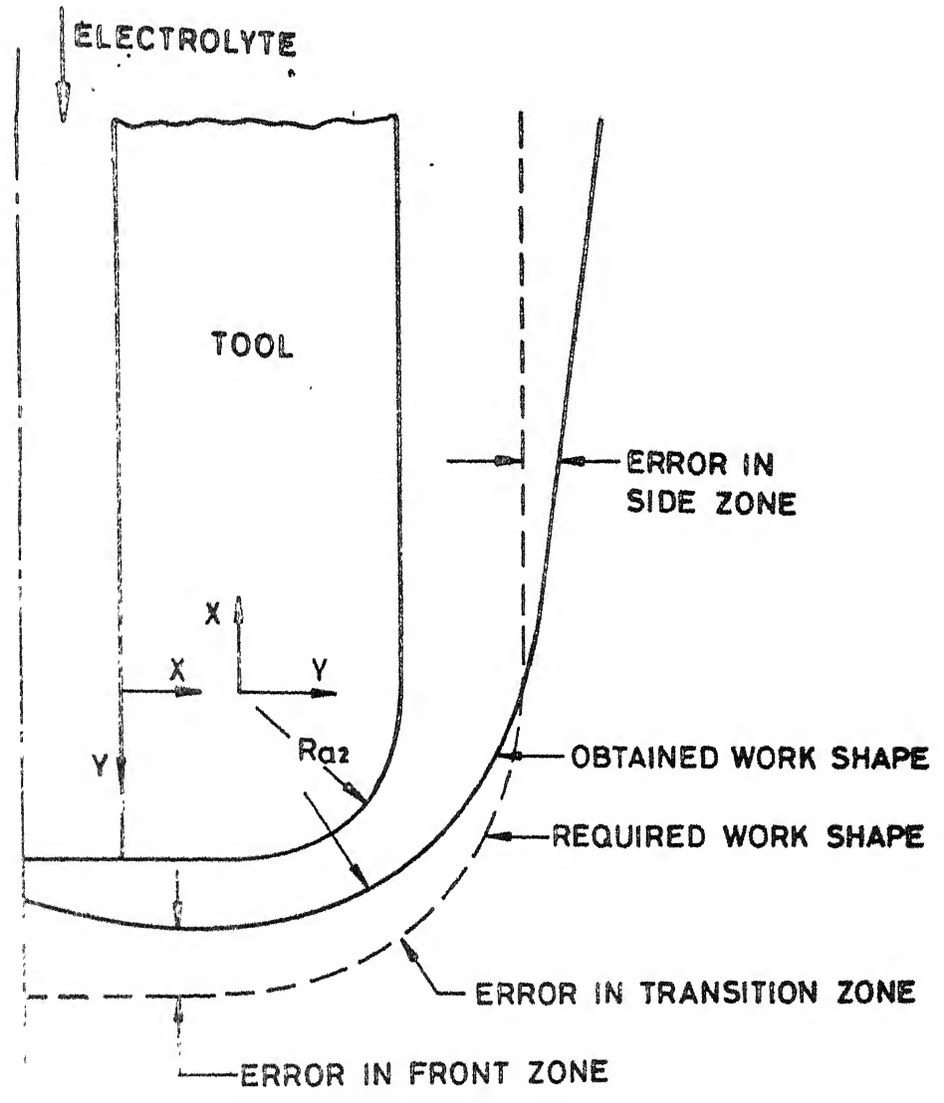

FIG. 4.1 ERROR REPRESENTATION IN ECD.

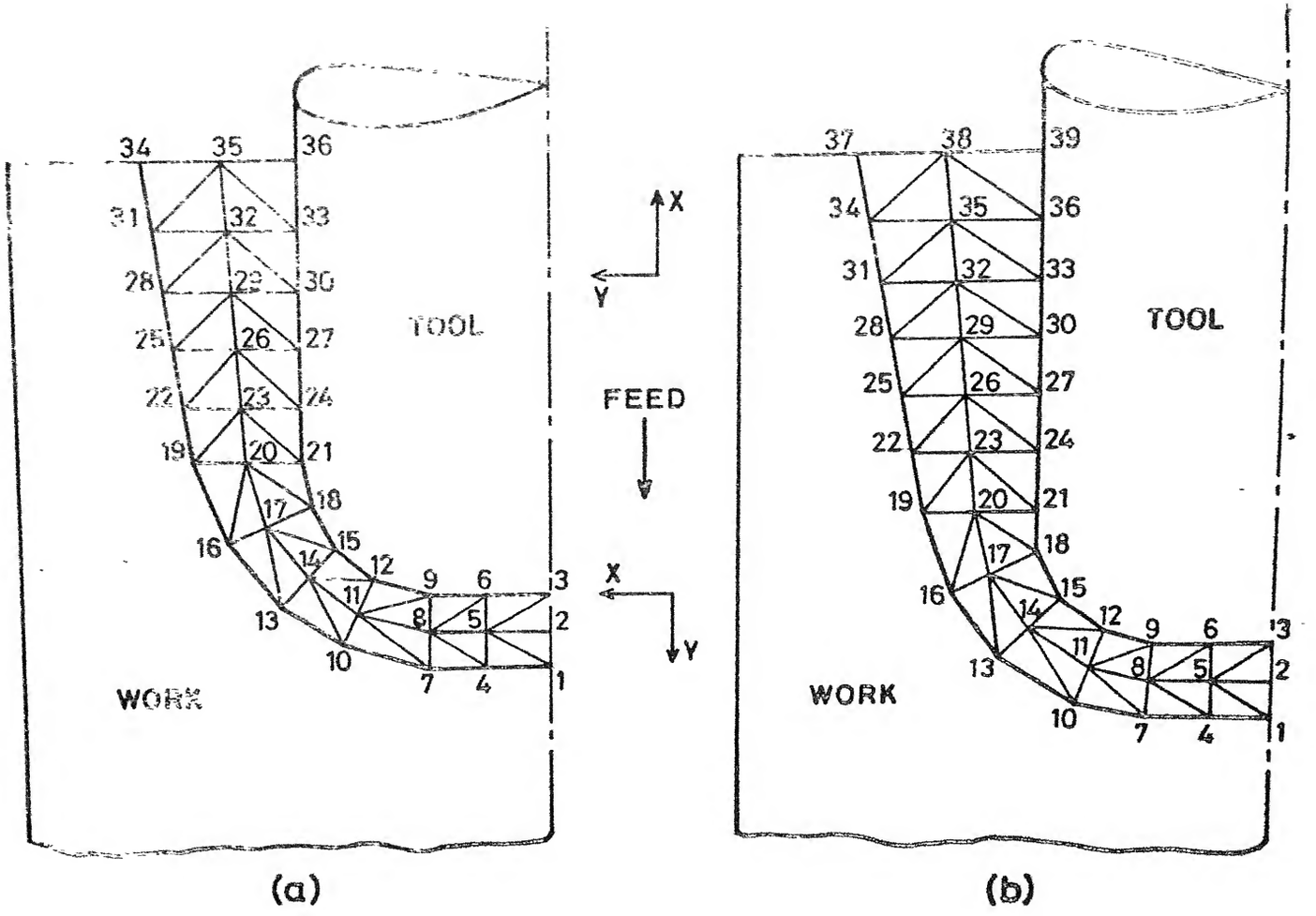

(a) (b)

FIG. 4.2 FINITE ELEMENT DISCRETIZATION OF IEG DURING ECD
(a) DURING i^{th} CYCLE (b) DURING $(i+1)^{th}$ CYCLE.

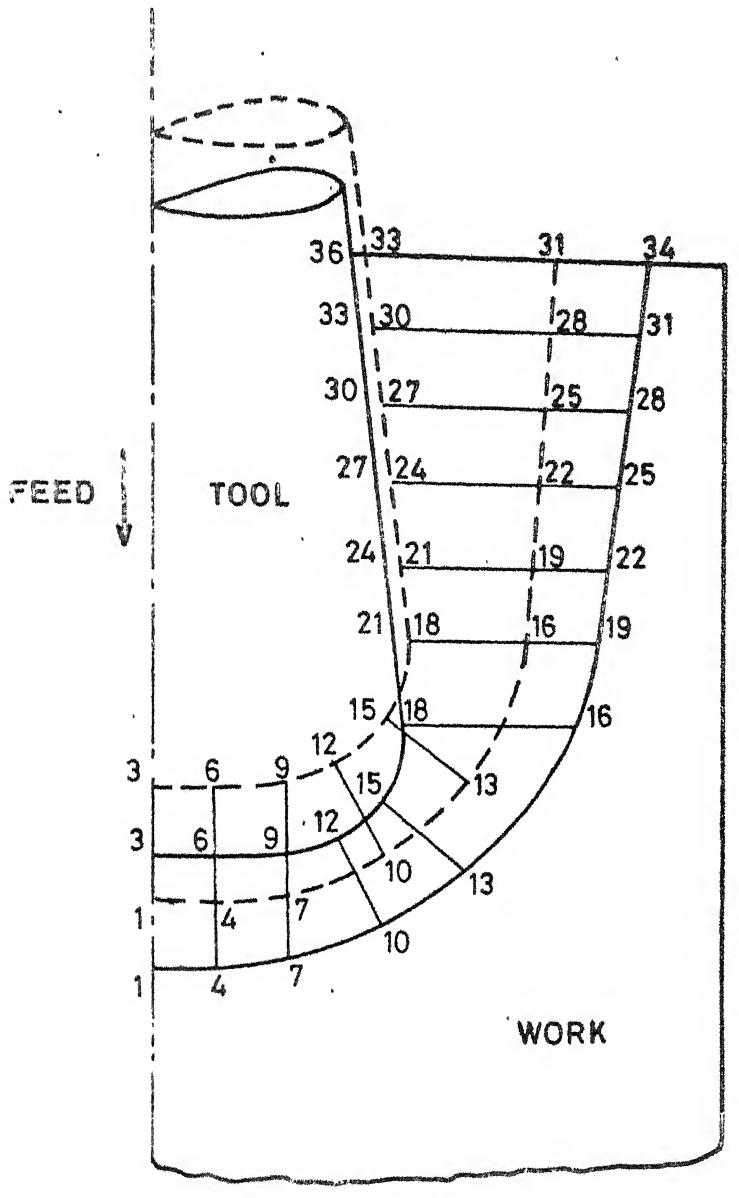

- - - - TOOL AND WORK SHAPES IN i^{th} CYCLE

——— TOOL AND WORK SHAPES IN $(i+1)^{th}$ CYCLE

FIG. 4.3 ANODE SHAPE PREDICTION DURING ECD.

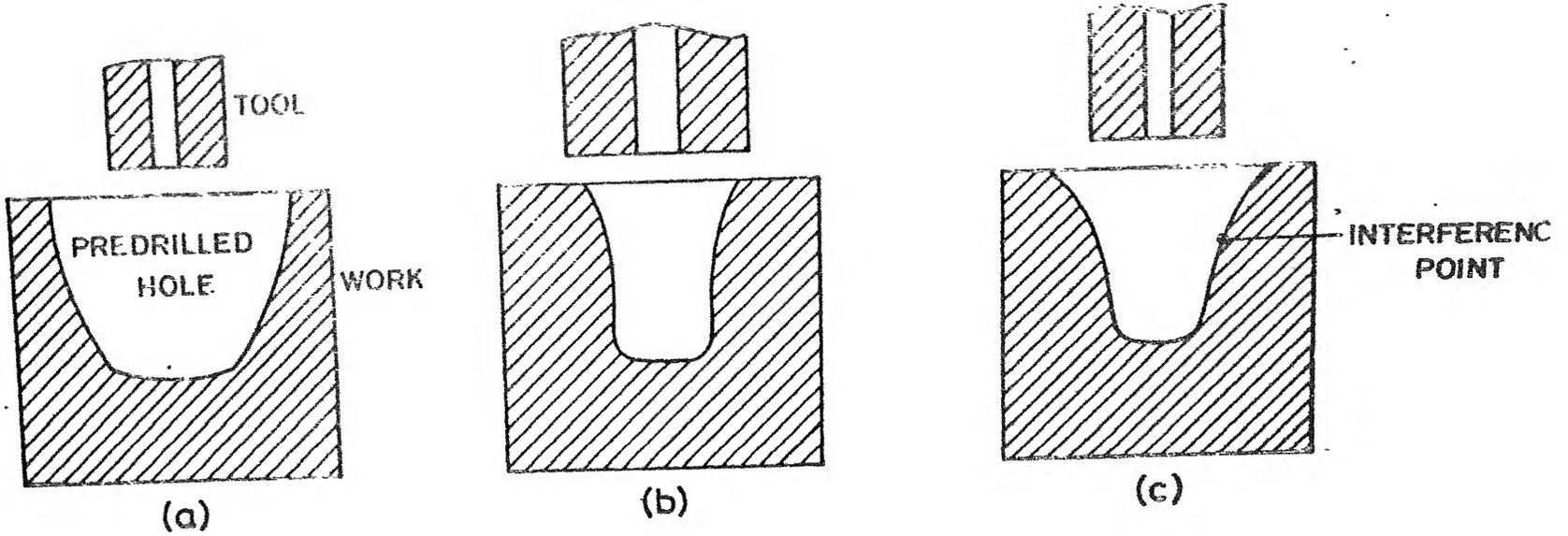

FIG. 4.4 DIFFERENT TYPES OF PREDRILLED HOLES ENCOUNTERED IN ECD

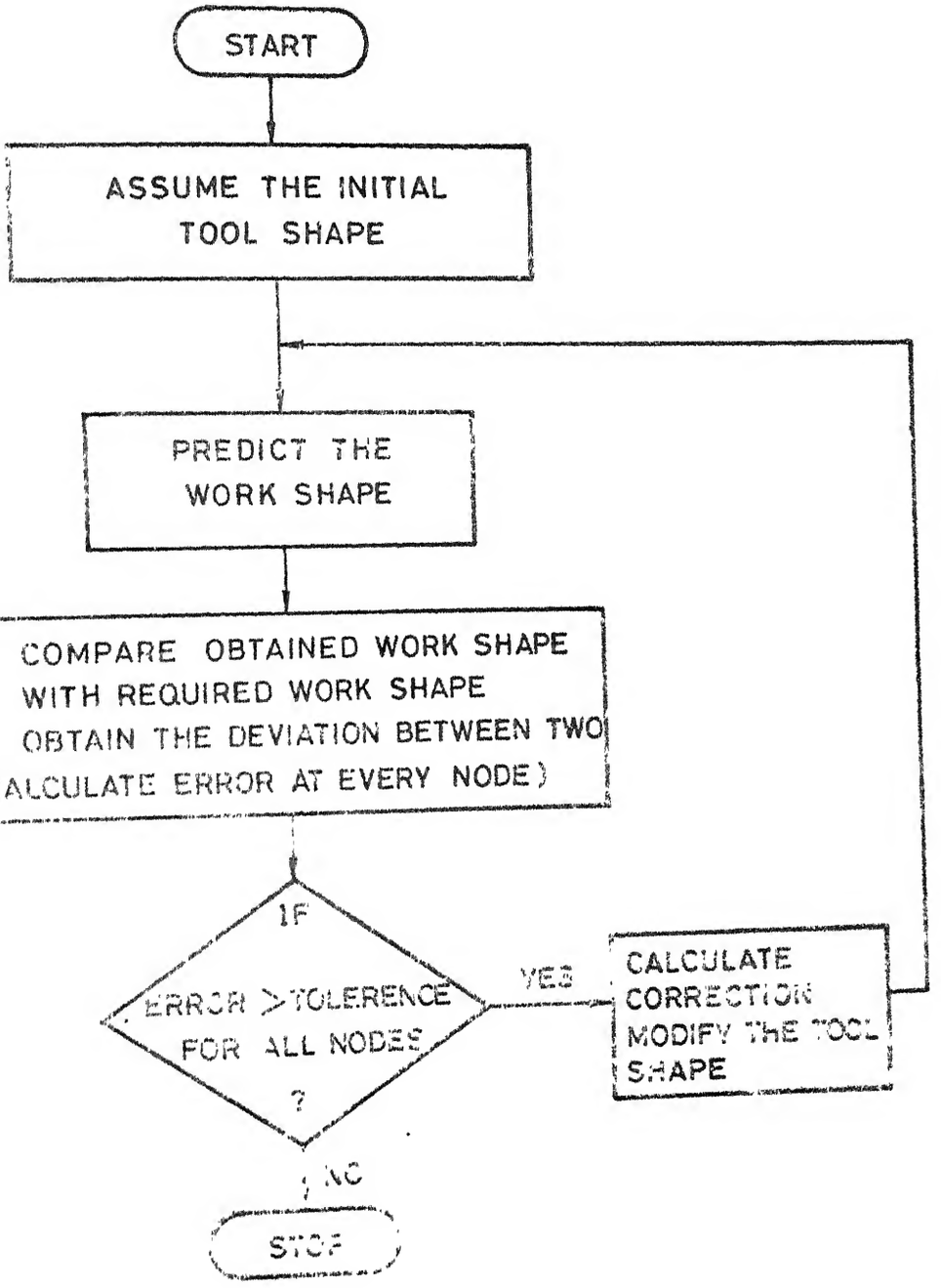

FIG. (3.3) FLOW CHART FOR GENERAL DESIGN PROCEDURE.

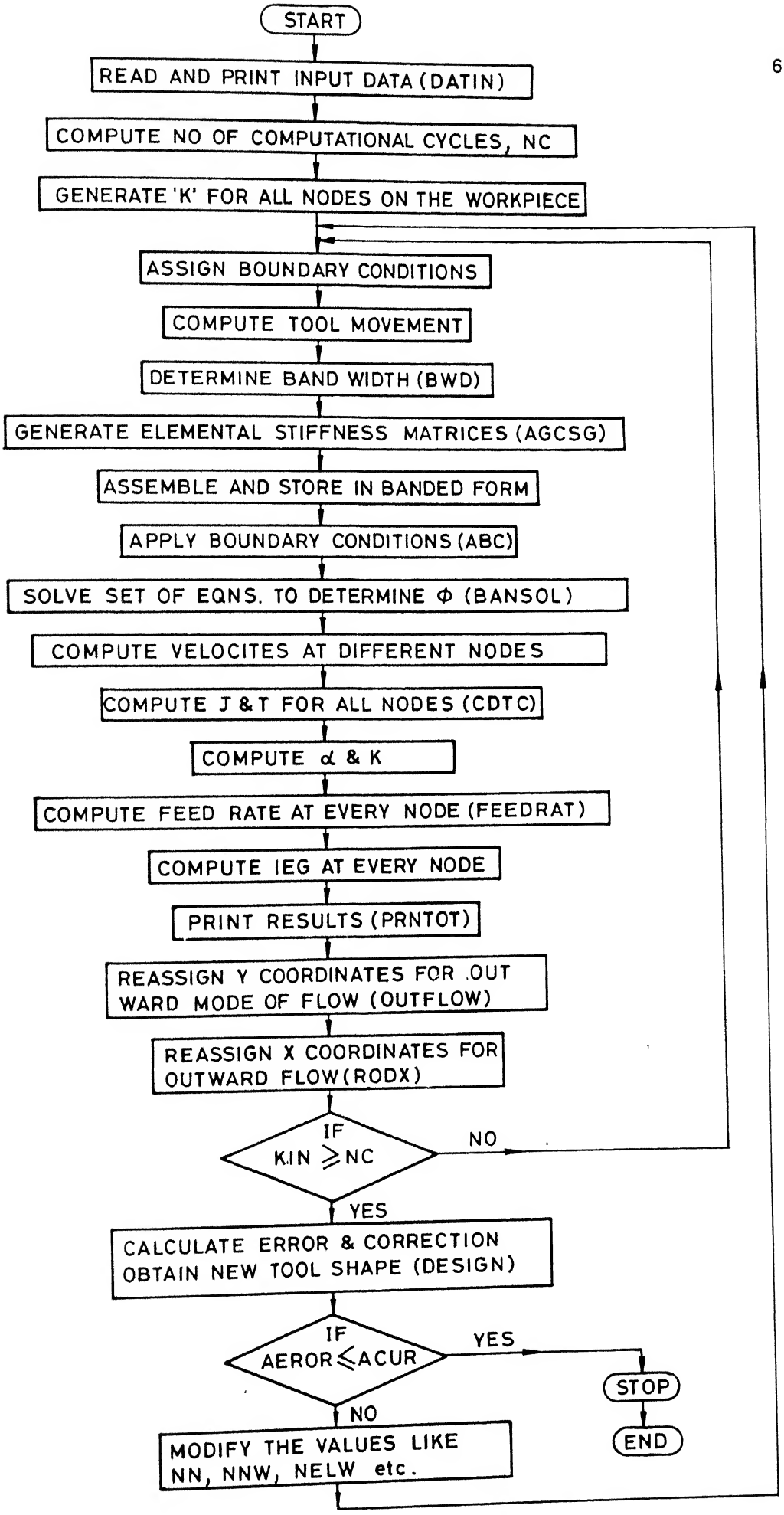

FIG 4.4(e) FLOW CHART FOR MODEL DES-22.

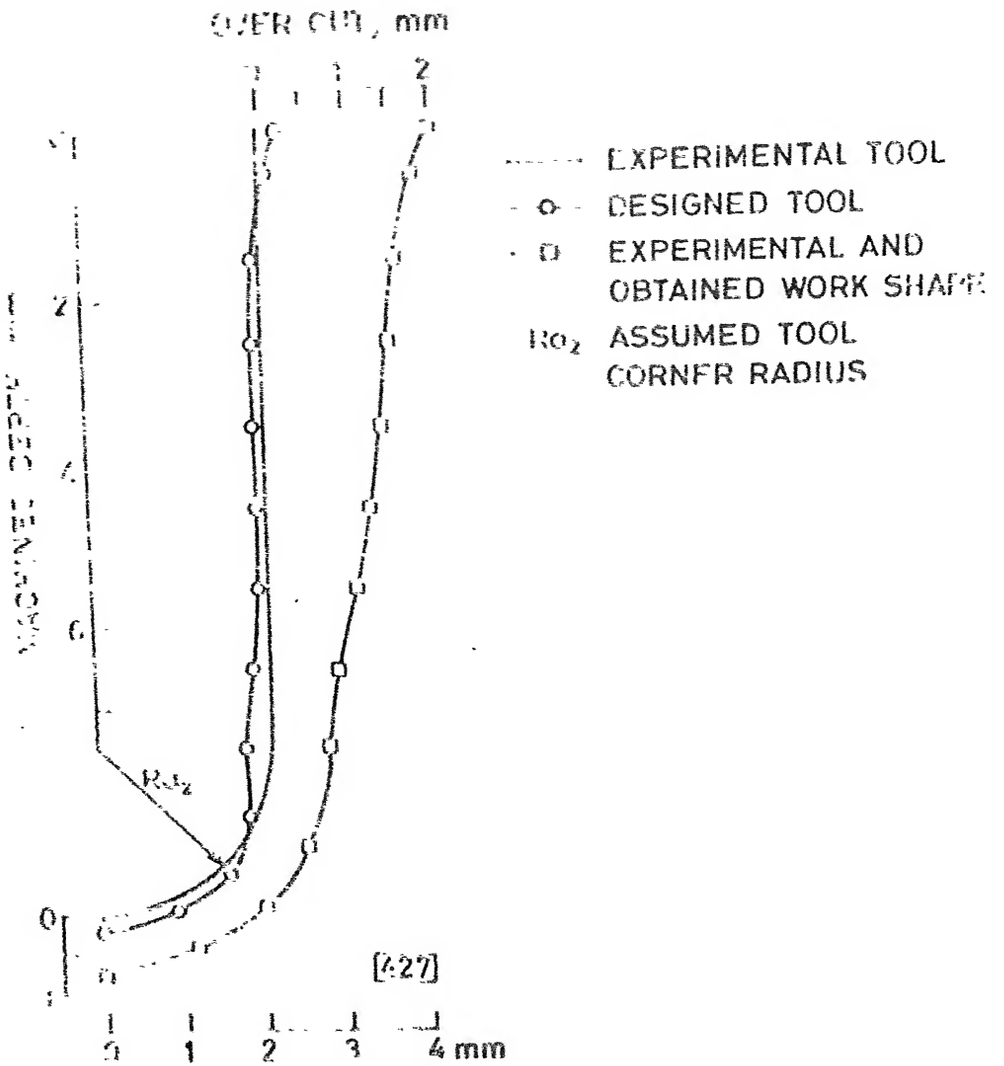
OVER CUT, mm
EXPERIMENTAL TOOL
DESIGNED TOOL
EXPERIMENTAL AND OBTAINED WORK SHAPE
Ra2 ASSUMED TOOL CORNER RADIUS
Ra2
427
0 1 2 3 4 mm

(a)

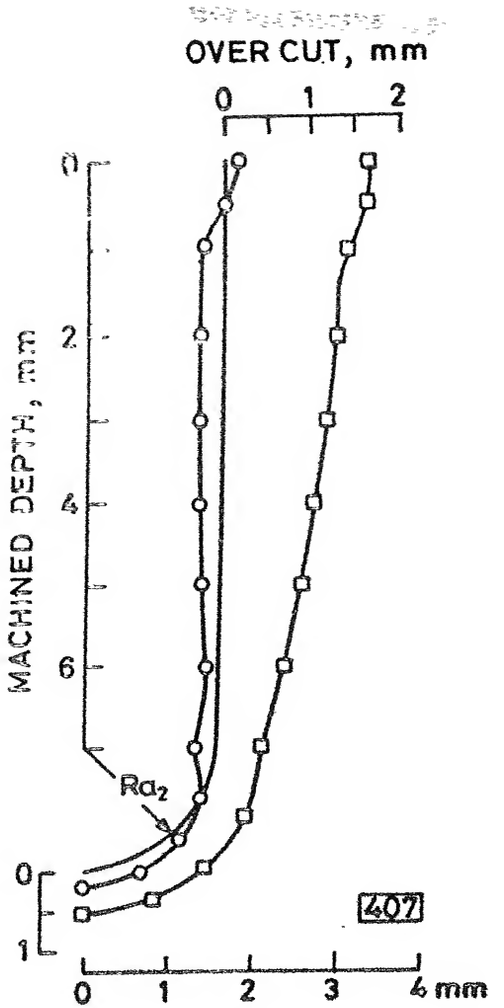
OVER CUT, mm
0 1 2
MACHINED DEPTH, mm
0 2 4 6
Ra2
407
0 1 2 3 4 mm

(b)

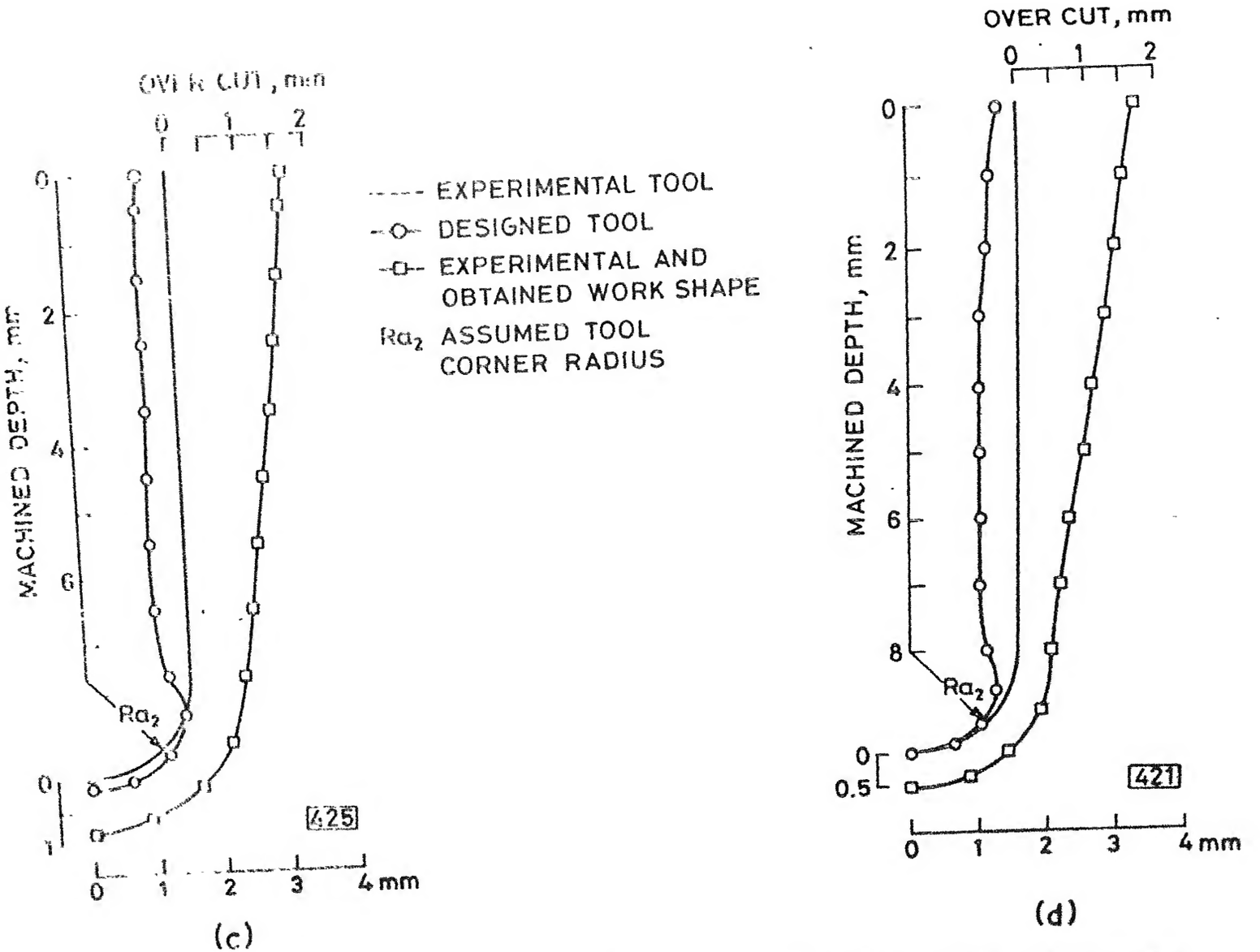

FIG. 4.5 COMPARISON OF EXPERIMENTAL AND DESIGNED TOOL PROFILES DURING ECD.

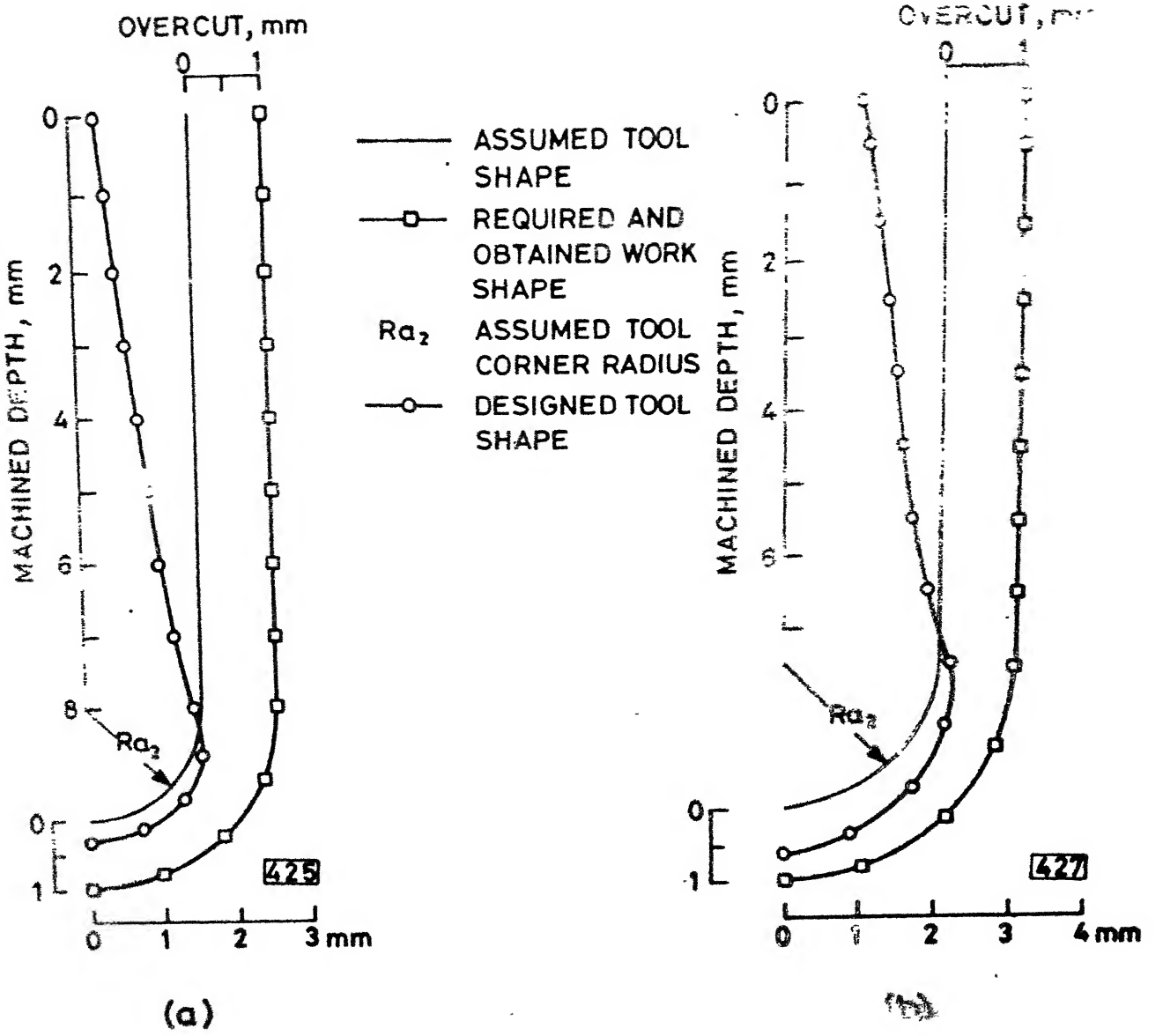
OVERCUT, mm
MACHINED DEPTH, mm
ASSUMED TOOL SHAPE
REQUIRED AND OBTAINED WORK SHAPE
Ra2 ASSUMED TOOL CORNER RADIUS
DESIGNED TOOL SHAPE
Ra2
425
427
3 mm
4 mm
(a)

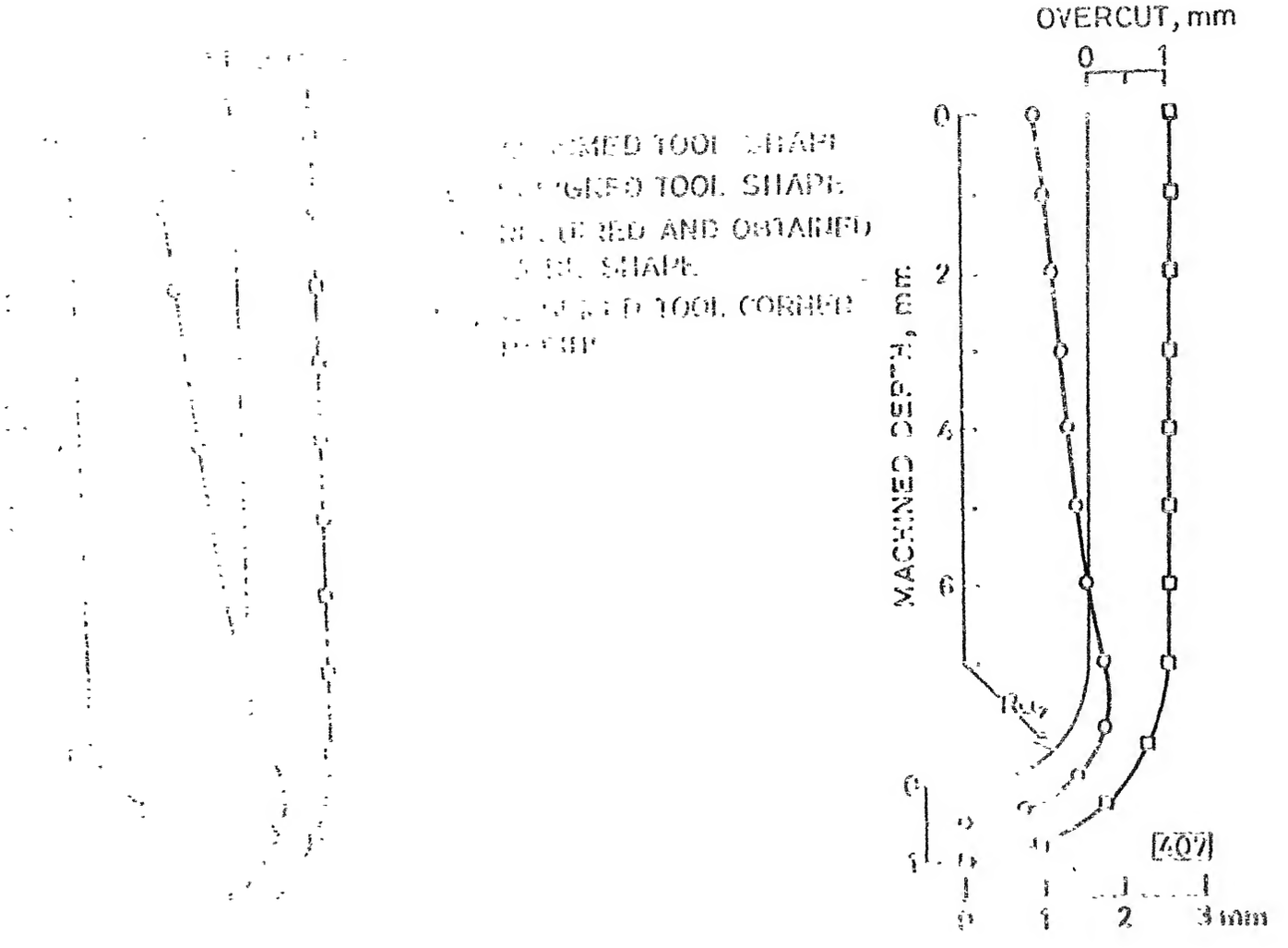

(d)

...D TO A SHAPE FOR STRAIGHT SIDE HOLE (ECD)

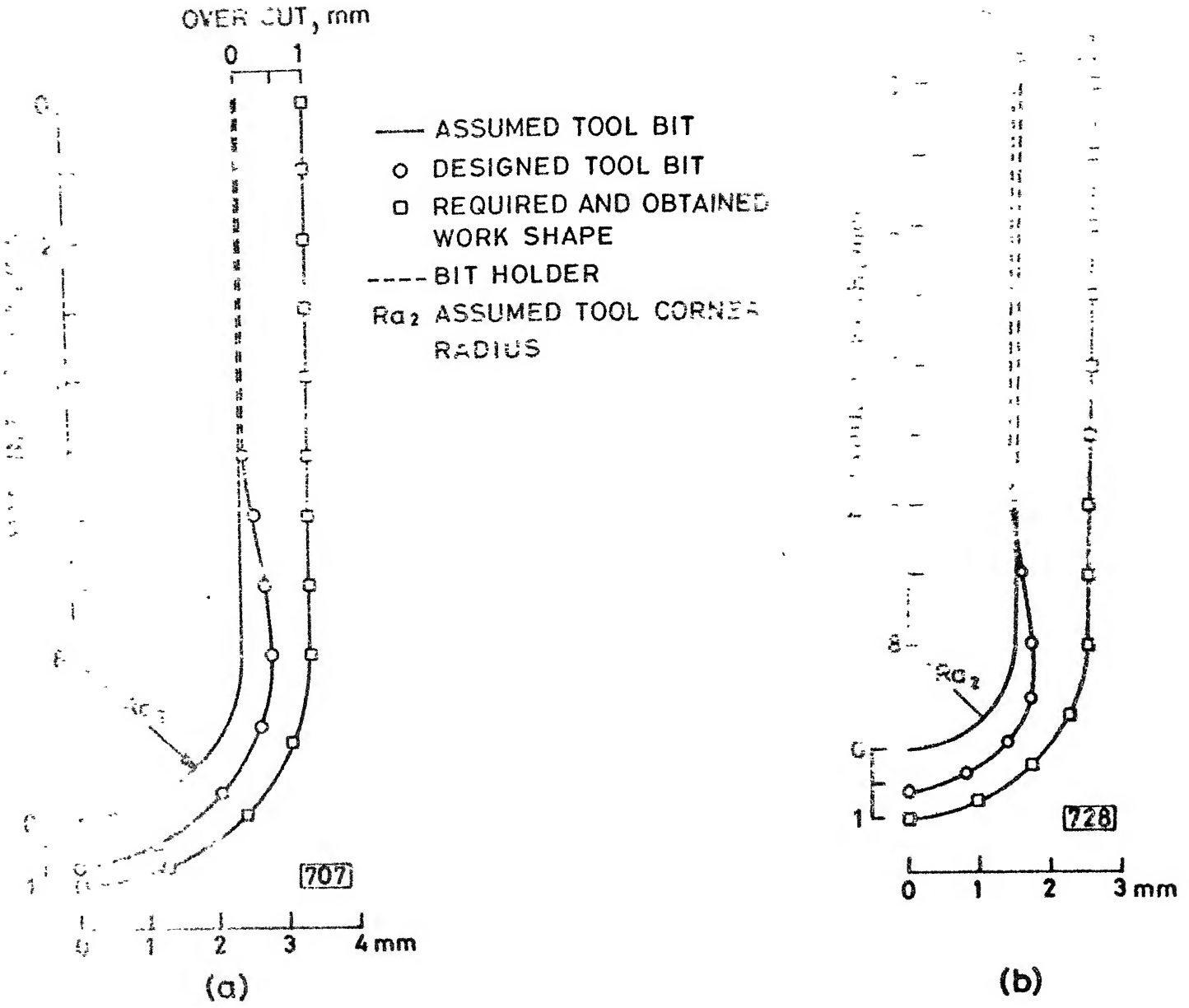

DESIGNED TOOL BIT FOR STRAIGHT SIDED HOLE (ECBD)

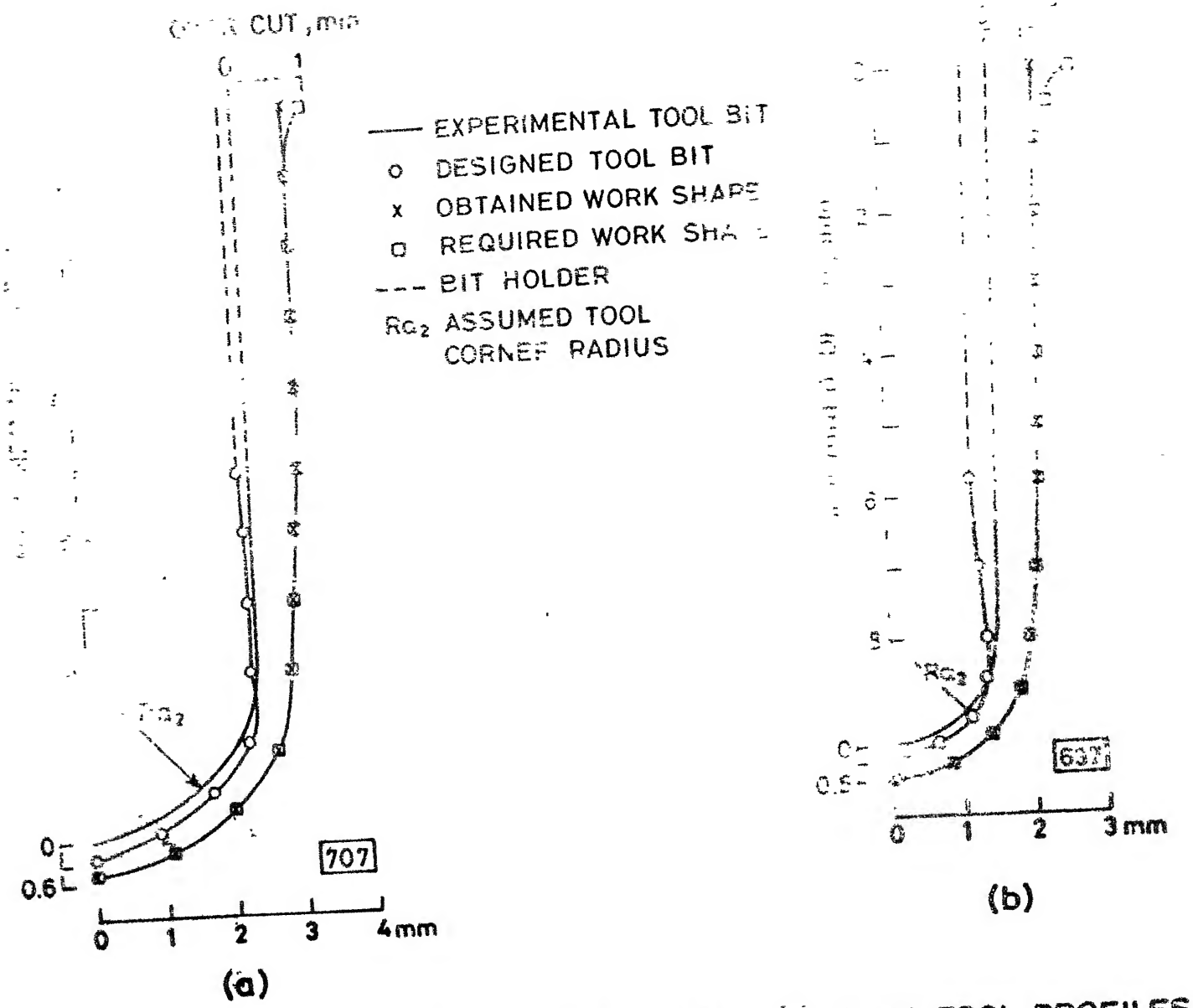

FIG. 4.8 COMPARISON OF EXPERIMENTAL AND DESIGNED TOOL PROFILES DURING ECBD.

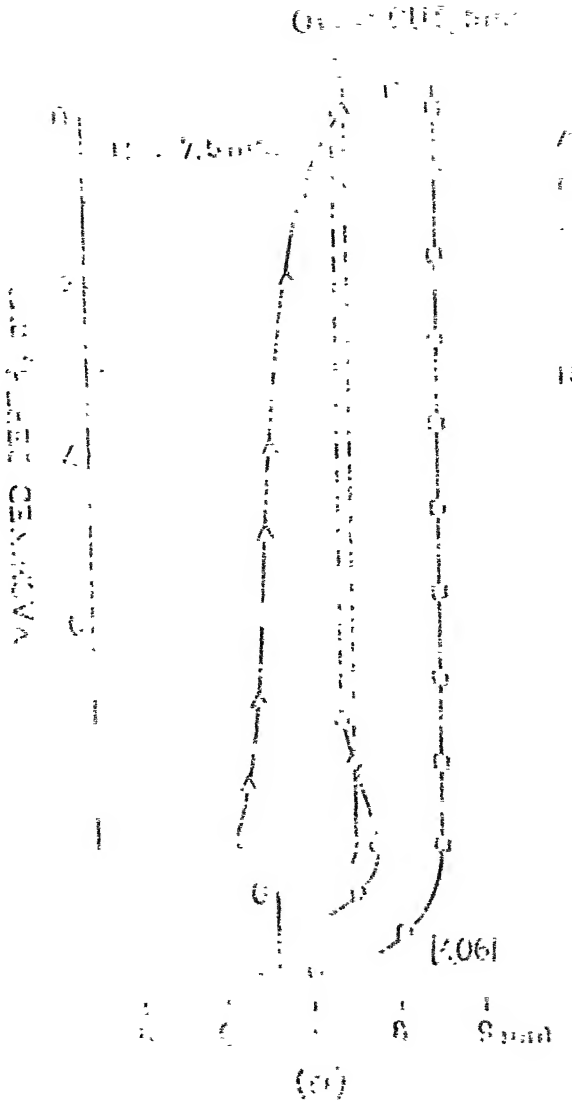

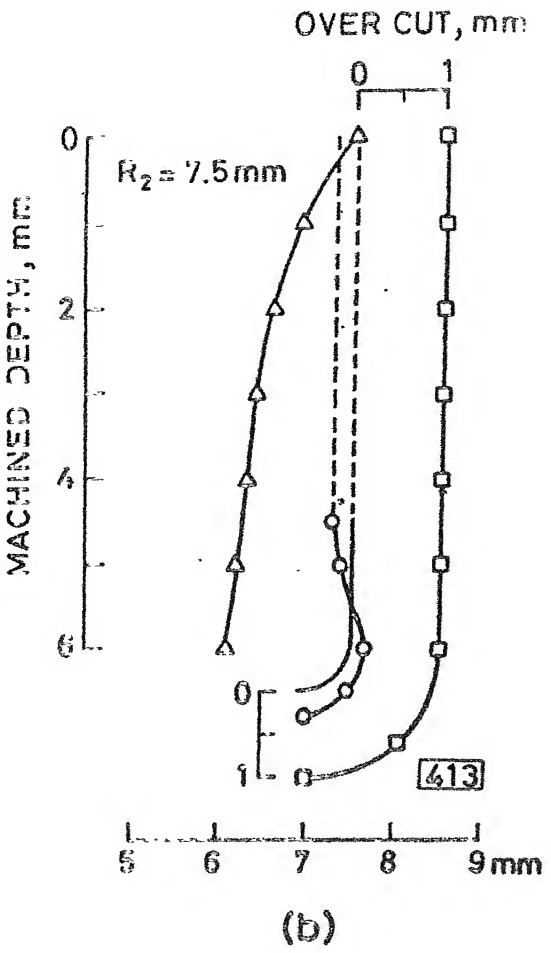

FIG 4.8 DESIGNED TOOL BIT FOR STRAIGHT SIDED HOLE (ECB)

CHAPTER V

SCOPE FOR FUTURE WORK

The work embodied in this thesis can be extended in the following directions:

(1) An attempt should be made to improve the accuracy of the designing model by improving the anode shape prediction model in the following ways,

   (a) The effect of the stray current attack on the anode profile should be considered.

   (b) More accurate electrolyte flow velocity distribution in IEG should be obtained by solving Navier-Stroke's equations.

(2) For the practical applications (for example, elliptical, parabolic, shape drilling, etc.) the tool design models based on three dimensional analysis should be evolved.

(3) This tool design procedure can be extended to external shaping as well.

(4) Desired work shape can be obtained from the given tool shape and machining conditions provided independent parameter like voltage or feed rate or both can be accurately controlled during the process. For the purpose of real time control of these parameters, microcomputer capabilities can be utilized. The beauty of the proposed method (Appendix-II) is to use the same tool for producing different shapes and sizes of workpieces.

Such analytical models can also be applied for the design of segmented tools (Figure A.4) whose shape and size will be changing with time according to the designed program.

REFERENCES

1. DeBarr, A.E. and Oliver, D.A., "Electrochemical Machining", Macdonald and Co. Ltd., 1968.

2. Thrope, J.F., "Hydraulic Aspects of ECM Tool Design", Society of Mfg. Engg., Creative Mfg. Seminar, Jan. 1976.

3. Koing, W. and Pahl, D., "Accuracy and Optimal Working Conditions in ECM", Annals CIRP, 1970, Vol. 18, pp. 223-230.

4. Tipton, H., "The Dynamics of ECM", Proc. 5th Int. Mach. Tool Des. Res. Conf., 1964, pp. 509-522.

5. Tipton, H., "Calculation of Tool Shape for ECM", (Ed. C.L. Faust), pp. 87-102.

6. Hopenfeld, J. and Cole, R.R., "ECM - Prediction and Correlation of Process Variables", Trans. ASME, Jl. of Engg. for Industry, Vol. 88, 1966, pp. 1-7.

7. Jain, V.K. and Pandey, P.C., "Tooling Design for ECM - A Finite Element Approach", Jl. of Engineering for Industry, Trans. ASME, May 1981, Vol. 103, pp. 183-190.

8. Jain, V.K., "An Analysis of ECM Process for Anode Shape Prediction", Ph.D. Thesis, University of Roorkee, India, 1980.

9. Jain, V.K. and Pandey, P.C., "Anode Profile in Electrochemical Drilling", Proc. 9th AIMTDR Conf. held at IIT Kanpur, 1980, pp. 338-350.

10. Jain, V.K. and Pandey, P.C., "Investigations into the Use of the Bits as a Cathode in ECM", Int. Jl. Mach. Tool. Des. Res., Vol. 22, 1982, pp. 341-352.

11. Murugan, S., "Prediction of Anode Profile in ECBD and ECBB Operations", M.Tech. Thesis, IIT, Kanpur, 1985.

12. Yogindra, P.G., "Two-Dimensional FE Analysis of Electrochemical Drilling Process for Anode Shape Prediction", M.Tech. Thesis, IIT, Kanpur, 1985.

13. Narayanan, O.H., Hinduja, S. and Noble, C.F., "The Prediction of Workpiece Shape During Electrochemical Machining by the Boundary Element Method", Int. Jl. Mach. Tool Des. Res., Vol. 26, No. 3, pp. 323-338, 1986.

14. Nilson, R.H. and Tsuei, Y.G., "Free Boundary Problem for the Laplace Equation with Application to ECM Tool Design", Jl. of Applied Mechanics (Trans. ASME), March 1976, pp. 54-58.

15. Nilson, R.H. and Tsuei, Y.G., "Inverted Cauchy Problem for the Laplace Equation in Engineering Design", Jl. Engg. Math., Vol. 8, 1974, pp. 329-337.

16. Lawrence, P., "Computer Aided Design for ECM Electrodes", IJMTDR, Vol. 21, 1981, pp. 379-385.

17. Idem, "Prediction of One Dimensional Equilibrium Cutting Gap in ECM", Ibid, Vol. 91, 1969, pp. 755-765.

18. Jain, V.K. and Pandey, P.C., "On the Heat Transfer Model for ECM Using Finite Element Technique", Proc. 5th National Heat and Mass Transfer Conf., Hyderabad, Feb. 1980, pp. 355-362.

19. Jain, V.K. and Murugan, S., "Investigations into the Effect of Cathode Material on Temperature Distribution During ECM", Int. Jl. Prodn. Res., 1986, Vol. 24, No. 2, pp. 439-450.

20. Kawafune, K., Mikoshiba, T. and Noto, K., "The Effect of Working Parameters on the Working Gap During ECM", Jl. of C.I.R.P., Vol. XVIII, pp. 305-317.

21. Bhatia, S.M., "Effect of Electrolyte Conductivity on the ECM Process Accuracy", M.Tech. Thesis, IIT, Bombay, 1971.

22. Bhatia, S.M., Dave, R.K. and Choubey, M., "Effect of Some Variables on ECM Accuracy", IE(I) Journal-ME, Vol. 58, Sept.-Nov. 1977, pp. 84-88.

23. Thrope, J.F. and Zerkle, R.D., "Analytical Determination of Working Gap in ECM", Int. Jl. Mach. Tool Des. Res., Vol. 9, 1969, pp. 131-144.

24. McGeough, J.A., "Principles of Electrochemical Machining", Chapman and Hall, London, 1974.

25. Rao, S.S., "The Finite Element Method in Engineering", Pergamon Press, 1982.

26. Reddy, M.S., "Computer Aided Design of Cathode for ECM", M.Tech. Thesis, IIT, Kanpur, 1986.

27. Patankar, S.V., "A Numerical Method for Conduction in Composite Materials, Flow in Irregular Geometries and Conjugate Heat Transfer", Proc. 6th Int. Heat Transfer Conf., Toronto, 1978, pp. 297-300.

APPENDIX I

COMPUTATIONAL DETAILS

A.1 HEAT TRANSFER

The flow chart for the model TFET22 is shown in Figure 3.5. The other computational details are as follows.

HEAT GENERATION ($\dot{H}$)

For a rectangular element of length 'dx', height 'y' and thickness 'B' in IEG (Figure A.1(a)) heat generated due to Ohmic heating,

$$H = I^2R = V^2/R = KV^2 \qquad (A.1)$$

But $$K = \frac{K_o.A}{y} = \frac{K_o.dx.B}{y} \qquad (A.2)$$

where A = cross sectional area perpendicular to the current flow.

Substituting eq. (A.2) in (A.1), the heat generated per unit volume for the element,

$$\dot{H} = H/y.B.dx = \frac{K\,V^2}{y^2} \qquad (A.3)$$

It is assumed that the heat generated per unit volume for all the triangular elements inside the rectangular element remains the same.

As the machining progresses, the work surface becomes tapered (Figure A.1(b)). In that case, the element 'EFGH' is approximated as rectangular element of height y which is given by,

$$y = (y_1 + y_2)/2 \qquad (A.4)$$

Again for all triangular elements inside the element 'EFGH', $\dot{H}$ is assumed to be the same, which is given by eq. (A.3).

BRIEF DESCRIPTION OF SUBROUTINES USED

(I) SUBROUTINE DATIN:

This subroutine reads in and prints out the input data.

(II) SUBROUTINE ABC:

This applies boundary conditions (specified voltages).

(III) SUBROUTINE BANSOL:

This solves the sparse, banded, symmetric matrix and gives the field potential distribution within the IEG.

(IV) SUBROUTINE ELEMAT:

This generates elemental conductivity, mass and heat generation matrices.

(V) SUBROUTINE ASEMBL:

This assembles elemental matrices into global form.

(VI) SUBROUTINE BELMAT:

This calculates boundary matrices.

(VII) SUBROUTINE BASMBL:

This assembles element boundary matrices into a global form.

(VIII) SUBROUTINE MATMUL:

This performs some matrix operations required for solving simultaneous linear, differential equations.

(IX) SUBROUTINE TBOUND:

This applies temperature boundary conditions.

(X) SUBROUTINE F04AF:

This is a system subroutine used for solving system of simultaneous linear equations.

(XI) SUBROUTINE CDTC:

This calculates current density (J), conductivity (K) at all the nodes.

(XII) SUBROUTINE INELGP:

This calculates IEG for the case of zero and finite feed rate conditions for a node at any instant of time 't'.

(XIII) SUBROUTINE BWD:

This determines value of bandwidth.

(XIV) SUBROUTINE ZER:

A subroutine that initialises the matrix.

A.2. TOOL DESIGN

Figure 4.4(e) shows the flow chart of the model DES22. Some computational details have been presented below.

While modifying the tool shape in the side zone, the correction has been applied in a direction perpendicular to the tool axis (along y, Figure A.2). But the correction at any node should be applied in a direction normal to the work surface at that node (along y_{ni}, Figure A.2), because the machining takes place in that direction. Further, any point 'p' (on the work surface), in the beginning of a computational cycle moves to 'p'' in a normal direction after that computational cycle (Figure A.2). The movement in the x-direction 'pQ' (Figure A.2) has been neglected in the anode shape prediction model.

From the Figure A.2,

$$pp' = \left[\frac{\eta JE}{F\rho_w} - f\cos\theta\right]\Delta t \qquad (A.5)$$

$$\text{x movement, } pQ = \left[\frac{\eta JE}{F \rho_w} - f\cos\theta\right] \Delta t \cos\theta \qquad (A.6)$$

$$\text{y movement, } p'Q = \left[\frac{\eta JE}{F \rho_w} - f\cos\theta\right] \Delta t \sin\theta \qquad (A.7)$$

Similarly, the point 'M' on the work surface moves to M' (Figure A.2) and so on. The line joining all such points like p', m', ... will give new work surface, after a computational cycle.

If a node 'o' on the tool moves to 'o'' in a computational cycle time of Δt sec. the new normal gap corresponds to o', y_n, is given by

$$y_n = y_{ni} + \left[\frac{\eta JE}{F \rho_w} - f\cos\theta\right] \Delta t \qquad (A.8)$$

where y_{ni} = initial normal gap (corresponds to 'o').

But, in the present model the point 'p' is assumed to move to 'p"' (and M to M" etc.) in the y-direction (Figure A.2). The new IEG at node o"' in the y-direction, y_o (p"o"'), is calculated as,

$$y_o = y_i + \left[\frac{\eta JE}{F \rho_w} - f\cos\theta\right] \Delta t \qquad (A.9)$$

where Y_i = initial IEG (o"'p) in the y-direction.

However, for very small computational cycle times (30 sec.), the tool movement (oo') will be very small. Therefore, the x-movement (eq. (A.6)) can be neglected. In this case the error incorporated by eq. (A.9) reduces to 'f cosθ t'. Even though this error is very small (for f = 0.006 mm/s, Δt = 30 s, $\theta = 88^\circ$, error = 0.002 mm), this goes on increasing as it is of repetitive nature.

For the clearence type of the predrilled hole, the front and transition zones have been neglected. The finite element discretization starts from the second computational cycle onwards as shown in Figure A.3. In this case, the current density for the first computational cycle is calculated using the following equation:

$$J = K(V - \Delta V)/r_w \ln(\frac{r_w}{r_t})$$

where r_w = radius of the work

r_t = radius of the tool.

In the anode shape prediction for the full interference type (Figure 4.4(b)) of predrilled holes, all the three zones are considered in the same way as in case of ECBD. For the partial interference type of predrilled holes (Figure 4.4(c)), the transition zone is considered from the interference point onwards.

For all the cases, the electrolyte flow velocity distribution is obtained by the continuity equation i.e. U = Q/A. But this is not accurate for the case of ECB.

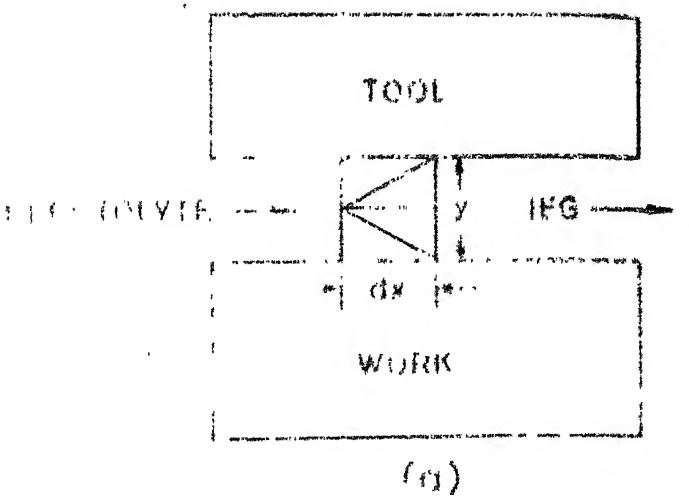

(a)

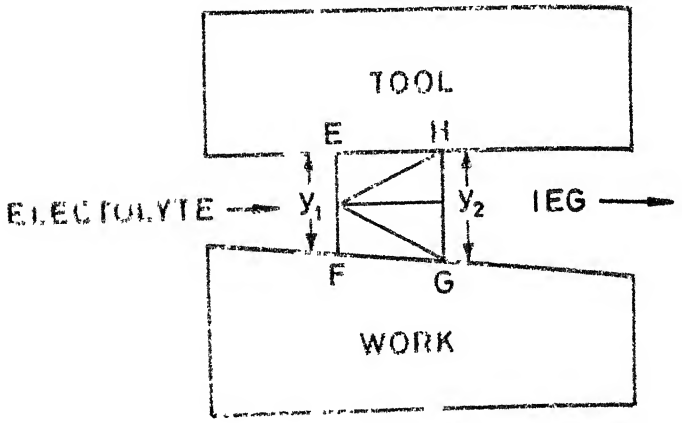

(b)

FIG. A1 HEAT GENERATION CALCULATION.

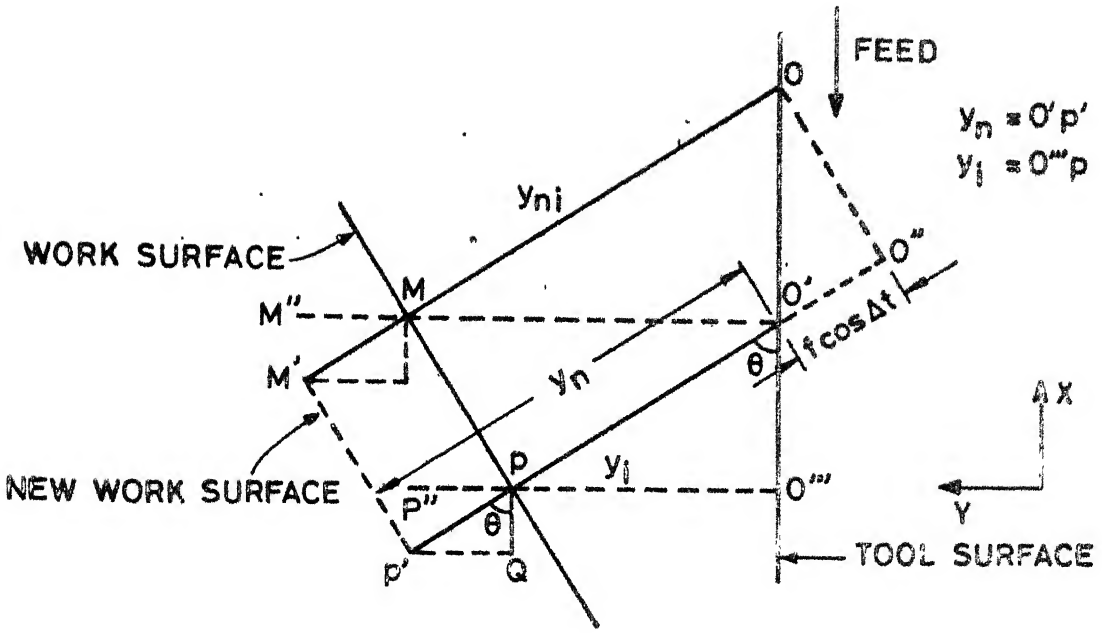

FIG. A2 ANODE SHAPE PRIDICTION IN SIDE ZONE.

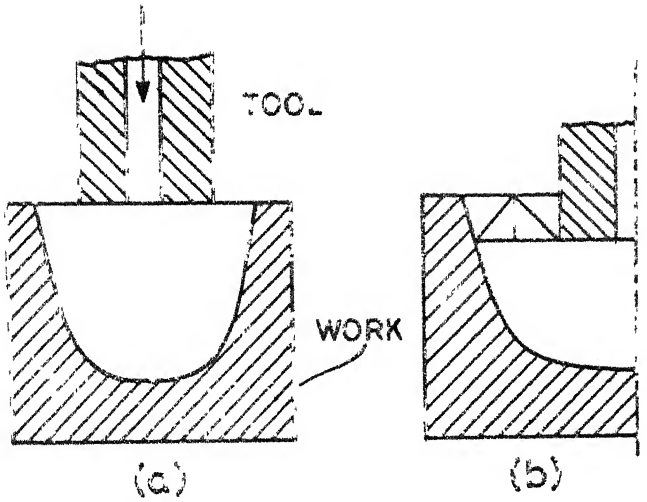

FIG. A3 ANODE SHPE PRIDICTION IN ECB

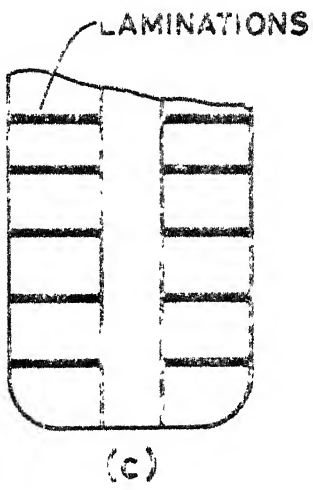

FIG. A4 LAMINATED TOOL.

APPENDIX II

TOOL DESIGN

Conventional ECM tool design starts with selecting optimum machining conditions. Next step is to predict tool shape for producing the required work shape, while machining under prescribed (or optimum) machining conditions. In the subsequent stages, the other design aspects like electrolyte flow path, insulation etc., are considered.

The tooling design problem can be attempted from the other direction also i.e. controlling the machining conditions for producing required work profile, while machining with a fixed tool geometry. Apart from the shape of the tool, the work profile mostly depends on the independent parameters like voltage, feed rate and machining time. For a fixed tool geometry, the desired work shape can be obtained by varying the voltage or feed rate. In case of voltage, the desired work shape can be obtained,

(1) by varying the voltage with time

(2) by varying the voltage along the tool.

Voltage can be varied easily with time by suitable means viz., by the use of microprocessor or adaptive controls. Figure A.5 shows the different analytical work profiles for different voltage variations (Figure A.5). The effect of voltage variation with time on work profile can be clearly seen from the Figure A.5.

Varying the voltage along the tool in a required fashion can be possible with the microprocessor and adaptive controls. In this case, the tool has to be made of number of small bits separated by very thin laminations of insulating material (Figure A.4).

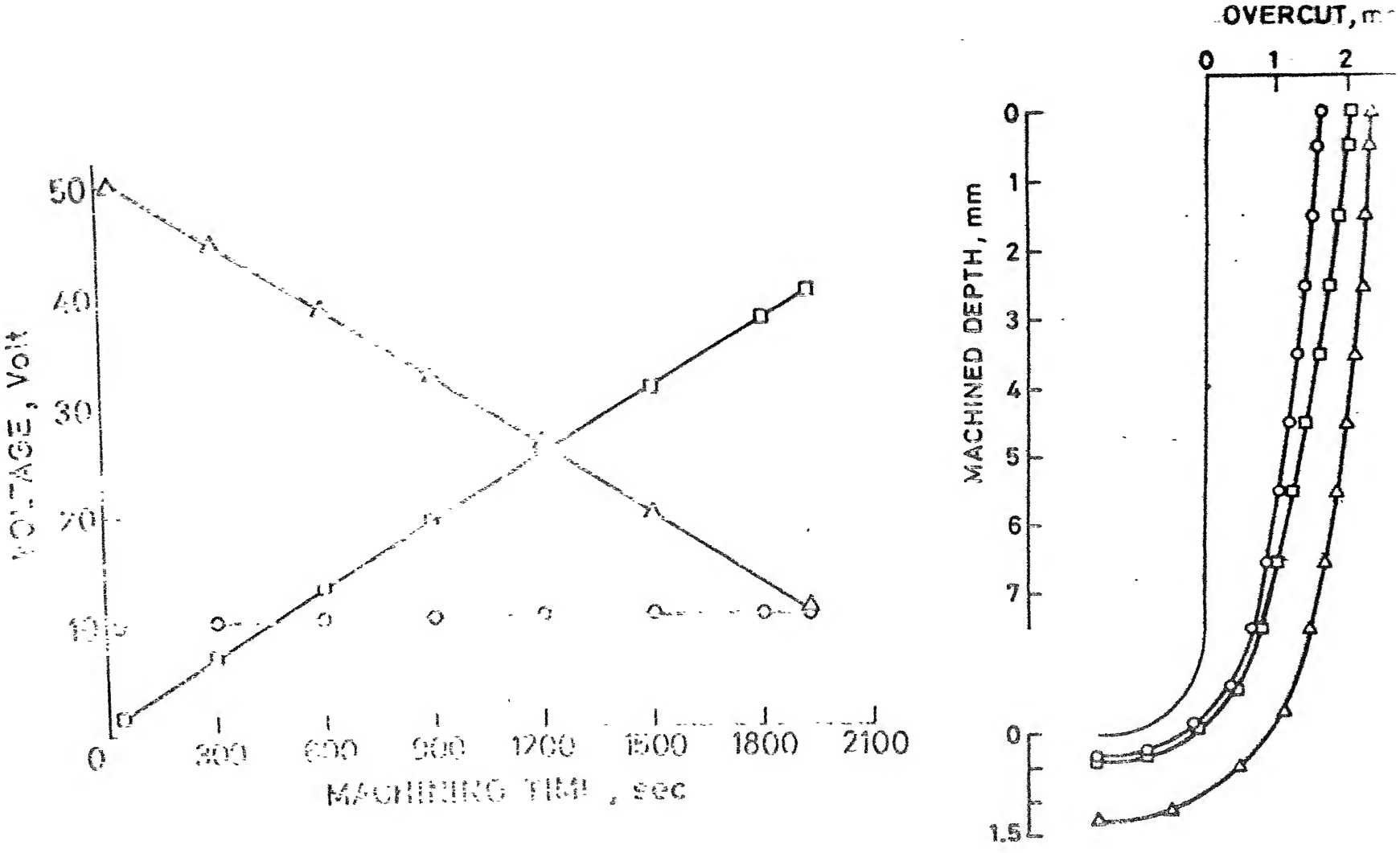

FIG. A5 ANODE PROFILES FOR DIFFERENT VOLTAGE VARIATIONS.

TABLE : 1

Thermal Properties of Tool, Work and Electrolyte

Material	K W/cm-°C	Density (ρ) gm/cm^3	Specific heat (C) WS/gm-°C
Copper	3.8	8.954	0.3831
Steel	0.6	7.81	0.46
Electrolyte	0.06	1.0	4.18

TABLE : 2

Experimental Conditions and Temperature Distribution during ECM with Plane Parallel Electrodes [22]

Total machining time = 300 sec., $K_o = 0.1412\ ^{-1}cm^{-1}$,

C = Copper, S = Stainless steel

Job No.	$\bar{E}_v$ (Volts)	f (mm/s)	Q (lit/min)	Y_o (mm)	Temperature at distance (°C)			
					X=2.5	=6.5	=17.5	=21.5 mm
C-1	12.0	0.64	1.5	0.60	37.2	39.3	42.0	43.0
S-1	12.0	0.64	1.5	0.60	32.3	34.7	40.9	42.0
C-2	16.0	0.64	0.9	0.82	36.2	36.3	39.8	41.0
S-2	16.0	0.64	0.9	0.82	32.3	33.6	39.5	40.8
C-3	20.0	0.64	2.1	1.10	34.2	36.0	38.3	40.8
S-3	20.0	0.64	2.1	1.10	32.3	34.7	38.3	40.8
C-4	12.0	0.88	1.4	0.50	37.3	39.8	42.1	44.0
S-4	12.0	0.88	1.4	0.50	31.3	33.7	-	36.7
C-5	16.0	0.88	1.5	0.60	37.3	39.8	45.6	48.0
S-5	16.0	0.88	1.5	0.60	32.5	35.0	-	45.6
C-6	20.0	0.88	1.7	0.75	37.3	39.8	44.0	46.8
S-6	20.0	0.88	1.7	0.75	32.3	34.7	42.0	45.0
C-7	12.0	1.13	1.3	0.40	42.1	44.0	49.1	50.4
S-7	12.0	1.13	1.3	0.40	34.8	-	46.6	52.5
C-8	16.0	1.13	1.4	0.50	46.6	50.1	53.6	57.1
S-8	16.0	1.13	1.4	0.50	34.8	39.5	-	53.6
C-9	20.0	1.22	1.6	0.65	46.7	47.9	53.7	57.1
S-9	20.0	1.22	1.6	0.65	36.0	39.5	52.0	56.0
C-10	12.0	1.22	3.0	0.60	30.3	31.5	32.8	35.2
S-10	16.0	1.22	1.4	0.50	36.2	39.8	52.6	58.4
C-11	16.0	0.64	3.2	0.84	31.5	-	35.2	36.3
S-11	12.0	1.22	1.2	0.40	33.8	-	46.3	51.5
C-12	20.0	0.64	3.1	1.10	32.5	33.8	36.2	39.9
S-12	20.0	1.22	1.6	0.60	38.3	40.8	53.6	61.7

TABLE : 3

Experimental Conditions used during ECD of Cast Low Alloy Steel [8]

$f = 0.00571$ mm/s, $Y_i = 1.0$ mm

Workpiece No.	K_i (ohm^{-1} mm^{-1})	$\bar{E}_v$ (Volts)	$\bar{I}_c$ (Amperes)	η %
Tool-1, $\bar{r}_t = 3.79$ mm, $\bar{r}_{tc} = 1.246$ mm, u = 5.69 m/s				
201	0.00790	14.348	12.52	83.70
413	0.00725	17.75	13.1	90.15
408	0.00725	15.31	16.24	91.70
409	0.00725	21.84	14.14	95.00
406	0.00725	12.94	13.28	86.9
Tool-3, $\bar{r}_t = 4.54$ mm, $\bar{r}_{tc} = 1.57$ mm, u = 5.263 m/s				
407	0.0063	12.93	15.0	93.16
421	0.0070	14.89	16.1	96.20
424	0.0060	18.5	19.86	92.0
425	0.0066	20.49	18.80	91.86
Tool-4, $\bar{r}_t = 5.03$ mm, $\bar{r}_{tc} = 2.13$ mm, u = 5.37 m/s				
429	0.0060	11.57	18.53	94.0
401	0.00547	12.975	22.15	91.82
418	0.00532	15.95	18.4	92.5
427	0.00532	17.62	-	-
5 402	0.00600	15.87	18.4	93.7

TABLE : 4

Machining Conditions used during ECBD and ECBB of Low Alloy Steel Castings and Low Alloy Steel Forgings [8]

$K_o = 0.0007\ ^{-1}\ mm^{-1}$, $Y_o = 1.0$ mm, Q = 5.37 litres/min

Job No.	$\bar{E}_v^*$ (Volts)	$\bar{I}_c$ (Amp.)	f ($\times 10^{-3}$), mm/s	r_t (mm)	r_{tc} (mm)	b_b (mm)	Total machining time (sec.)
627	3.88	25.67	3.70	8.9	0.5	5.0	2400
635	7.36	17.70	4.50	6.0	0.5	4.0	2400
637	7.64	17.17	6.19	5.5	1.5	3.8	2400
721	6.18	17.02	5.33	6.0	0.5	3.0	2400
725	7.55	13.80	3.70	6.00	0.5	3.0	2400
733	7.60	16.70	4.50	6.0	0.5	6.0	2400
735	6.75	19.41	5.33	6.0	0.5	5.0	2400
736	6.47	15.75	4.50	6.0	0.5	2.0	2400
737	7.33	16.50	4.50	6.0	2.3	5.2	2160
406	7.30	13.66	4.50	5.5	0.5	2.0	2400
413	8.07	12.79	4.50	5.5	0.5	2.0	1800
414	6.30	15.77	5.33	5.5	0.5	3.0	2400
424	6.77	15.07	6.18	5.5	0.5	3.0	2400

* - Inclusive over potential.

TABLE : 5

Experimental Observations About Overcut Inside Zone during ECD [8]

Job No.	Overcut, mm					
Depth X, mm	413	407	421	425	418	427
0.0	2.49	1.79	1.71	2.26	2.34	2.32
0.5	-	-	1.54	1.76	-	1.73
1.0	1.9	1.37	1.56	1.695	1.93	1.65
1.5	1-	-	1.4	1.61	-	1.63
2.0	1.61	1.26	1.45	1.6	1.64	1.44
2.5	-	-	1.31	1.51	-	1.51
3.0	1.42	1.17	1.36	1.52	1.475	1.34
3.5	-	-	1.13	-	-	1.42
4.0	1.27	1.05	1.25	1.43	1.36	1.12
4.5	-	-	1.02	1.33	-	1.31
5.0	1.16	0.94	-	1.34	1.25	1.02
5.5	-	-	0.91	1.23	-	1.18
6.0	1.1	0.84	0.92	1.11	1.13	0.91
6.5	-	-	0.71	1.1	-	1.03
7.0	0.96	0.66	0.715	0.91	0.98	0.61
7.5	-		-	0.84	-	0.61
8.0	0.35		0.60		0.725	-
8.5	0.62					

TABLE : 6

Experimental Observations about Overcut Inside Zone during ECBD and ECBB ("8").

Job No.	627	637	707	406	413
Depth in mm	Overcut, mm				
0.0	1.060	1.335	0.87	2.00	2.01
0.5	1.015	0.825	0.655	-	-
1.0	0.895	-	0.785	1.59	1.41
1.5	0.980	0.675	0.655	-	-
2.0	0.825	-	0.78	1.36	1.2
2.5	0.945	0.670	0.645	-	-
3.0	0.735	-	0.765	1.21	0.95
3.5	0.780	0.6725	0.655	-	-
4.0	0.650	-	0.765	1.10	0.75
4.5	0.665	0.665	0.65	-	-
5.0	0.565	-	0.765	1.02	0.66
5.5	0.555	0.65	0.65	-	-
6.0	0.440	-	0.725	0.95	0.55
6.5	0.400	0.64	0.625	-	-
7.0	0.350	-	0.61	0.88	0.5
7.5		0.59	0.505	-	
8.0		0.54	0.475	0.79	
8.5		0.49		-	
9.0				0.62	